J. Fluid Mech. (2014), *vol.* 757, *pp.* 251–296.
doi:10.1017/jfm.2014.489

Non-Newtonian stress, collisional dissipation and heat flux in the shear flow of inelastic disks: a reduction via Grad's moment method

Saikat Saha[1] **and Meheboob Alam**[1,†]

[1]Engineering Mechanics Unit, Jawaharlal Nehru Centre for Advanced Scientific Research, Jakkur P.O., Bangalore 560064, India

(Received 28 January 2014; revised 30 June 2014; accepted 21 August 2014; first published online 19 September 2014)

The non-Newtonian stress tensor, collisional dissipation rate and heat flux in the plane shear flow of smooth inelastic disks are analysed from the Grad-level moment equations using the anisotropic Gaussian as a reference. For steady uniform shear flow, the balance equation for the second moment of velocity fluctuations is solved semi-analytically, yielding closed-form expressions for the shear viscosity μ, pressure p, first normal stress difference $\mathscr{N}_1$ and dissipation rate $\mathscr{D}$ as functions of (i) density or area fraction ν, (ii) restitution coefficient e, (iii) dimensionless shear rate R, (iv) temperature anisotropy η (the difference between the principal eigenvalues of the second-moment tensor) and (v) angle ϕ between the principal directions of the shear tensor and the second-moment tensor. The last two parameters are zero at the Navier–Stokes order, recovering the known exact transport coefficients from the present analysis in the limit $\eta, \phi \to 0$, and are therefore measures of the non-Newtonian rheology of the medium. An exact analytical solution for leading-order moment equations is given, which helped to determine the scaling relations of R, η and ϕ with inelasticity. We show that the terms at super-Burnett order must be retained for a quantitative prediction of transport coefficients, especially at moderate to large densities for small values of the restitution coefficient ($e \ll 1$). Particle simulation data for a sheared inelastic hard-disk system are compared with theoretical results, with good agreement for p, μ and $\mathscr{N}_1$ over a range of densities spanning from the dilute to close to the freezing point. In contrast, the predictions from a constitutive model at Navier–Stokes order are found to deviate significantly from both the simulation and the moment theory even at moderate values of the restitution coefficient ($e \sim 0.9$). Lastly, a generalized Fourier law for the granular heat flux, which vanishes identically in the uniform shear state, is derived for a dilute granular gas by analysing the non-uniform shear flow via an expansion around the anisotropic Gaussian state. We show that the gradient of the deviatoric part of the kinetic stress drives a heat current and the thermal conductivity is characterized by an anisotropic second-rank tensor, for which explicit analytical expressions are given.

Key words: granular media, kinetic theory, rheology

†Email address for correspondence: meheboob@jncasr.ac.in

1. Introduction

A driven system of macroscopic or non-Brownian particles (e.g. driven by external vibration or shearing) resembles a molecular gas in which the particles move around randomly but lose energy upon collision, with the latter being a major difference between a granular gas and its molecular counterpart. Such a non-equilibrium state of agitated particles is also known as a rapid granular fluid (Goldhirsch 2003), for which the dense-gas kinetic theory (Chapman & Cowling 1970) has been appropriately modified and successfully used for a variety of flow configurations over the past three decades (Savage & Jeffrey 1981; Jenkins & Richman 1985*a*,*b*; Brey *et al.* 1998; Sela & Goldhirsch 1998; Brilliantov & Pöschel 2004; Rao & Nott 2008). In this paper we investigate the non-Newtonian rheology of a sheared granular system via kinetic theory. For an N-particle system, the stress tensor has contributions from both kinetic and collisional mechanisms of transport:

$$\boldsymbol{P} = \boldsymbol{P}_{kin} + \boldsymbol{P}_{coll}. \tag{1.1}$$

The first mechanism is dominant in the dilute regime, whereas the second one dominates in the dense regime. This can be further decomposed as

$$\boldsymbol{P} = p\boldsymbol{I} + \widehat{\boldsymbol{P}}, \tag{1.2}$$

where $p \equiv P_{ii}/\mathrm{dim}$ is the isotropic pressure (dim is the dimension), $\boldsymbol{I}$ is the identity tensor and the deviatoric stress is $\widehat{\boldsymbol{P}}$. The off-diagonal components of $\widehat{\boldsymbol{P}}$ are related to shear viscosity, which, in general, depends on the deformation rate. At the Navier–Stokes (NS) order, the stress tensor is Newtonian (i.e. linear in the shear rate, with the proportionality constant being the shear viscosity) and its diagonal components are equal. The latter implies that the first and second normal stress differences, $\mathscr{N}_1 \sim P_{xx} - P_{yy}$ and $\mathscr{N}_2 \sim P_{yy} - P_{zz}$, respectively, are identically zero. The non-zero normal stresses and/or the shear-rate dependence of viscosity are signatures of the non-Newtonian rheology of the medium. In kinetic theory, the normal stresses appear at the Burnett order (Burnett 1935; Grad 1949; Chapman & Cowling 1970) and hence cannot be taken into account in the standard NS-order hydrodynamic equations. Higher-order theories such as the Burnett equations (Burnett 1935; Sela & Goldhirsch 1998) or Grad's 13-moment equations (Grad 1949; Jenkins & Richman 1985*a*,*b*; Torrilhon & Struchtrup 2004) should therefore be used to correctly model the nonlinear rheology of granular fluids. Although the rest state of the Burnett equations is known to be unstable for molecular gases, there are ways to regularize these equations (Rosenau 1989). Moreover, it has been established recently (Santos 2008) that the partial sum of the shear stress converges in the uniform shear of a granular fluid, with its radius of convergence increasing with increasing dissipation or inelasticity. On the other hand, in Grad's method the distribution function is expanded in a Hermite series around the local Maxwellian of thermal equilibrium, and the moment equations for an extended set of hydrodynamic fields are written down.

The sheared granular fluid is known to possess finite normal stress differences for the whole range of densities (Sela & Goldhirsch 1998; Alam & Luding 2003*a*,*b*, 2005*a*,*b*) and the rate dependence of viscosity seems to be an inherent feature of the uniform shear state of a granular fluid (Santos, Garzo & Dufty 2004). Figure 1 indicates that the first normal stress difference is finite in a sheared granular fluid for a range of densities and its magnitude increases with increasing dissipation. Detailed

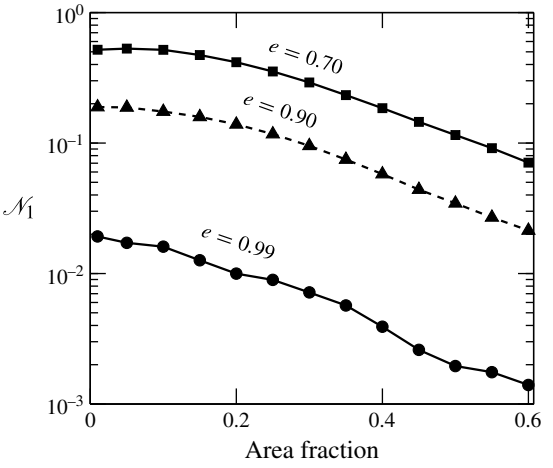

FIGURE 1. Variation of the first normal stress difference $\mathscr{N}_1 = 2(P_{xx} - P_{yy})/(P_{xx} + P_{yy})$ (see (4.21)) with area fraction of particles for different values of the restitution coefficient e. Data (symbols) correspond to event-driven simulations (Alam & Luding 2003*a*,*b*) for a sheared system of smooth inelastic hard disks with Lees–Edward boundary condition (see § 5.2 for details); lines are drawn to guide the eye.

simulations in two dimensions, i.e. for disks (Alam & Luding 2003*a*,*b*), and three dimensions, i.e. for spheres (Alam & Luding 2005*a*,*b*), have uncovered the following distinguishing features of normal stresses in a sheared granular fluid: (i) the first normal stress difference is positive in the dilute limit and undergoes a sign reversal at a finite density near the freezing point (depending on dissipation) in the dense limit; and (ii) the second normal stress difference is negative in the dilute limit and becomes positive beyond a moderate density. Both theory and simulation suggest that the magnitudes of the first and second normal stress differences increase with increasing dissipation.

Large normal stresses, such as those in figure 1, must be taken into account to correctly model a dissipative granular fluid in the rapid shear regime. Jenkins & Richman (1988) have incorporated normal stresses in their study of steady uniform shear flow (USF) of inelastic disks, following earlier kinetic theory work of Goldreich & Tremaine (1978) and Araki & Tremaine (1986) that used the anisotropic Gaussian as a reference state. They solved the second-moment balance equation in the two extreme limits of density, and derived analytical results for the stress tensor in dilute and dense flows, but the solutions for the full range of densities remain unexplored for the shear flow of inelastic disks. Chou & Richman (1998) analysed the USF of inelastic spheres and provided numerical solutions for the stress tensor for the full range of densities. More recently, Lutsko (2004) used an arbitrary Gaussian as a reference to solve the Enskog equation for a polydisperse mixture of inelastic hard spheres via the Hermite expansion (Grad 1949) around the anisotropic reference state, and the related kinetic integrals were simplified using a generating function technique. Focusing attention on the uniform shear state, he evaluated the stress tensor numerically and confirmed the previous numerical results of Chou & Richman (1998). It was further shown that the moment theory predictions for normal stress differences agree well with those obtained from the direct simulation Monte Carlo (DSMC) solution of the Enskog equation for a range of densities but can differ considerably

from molecular dynamics simulations of the same system for moderately dense binary mixtures. The reason for the latter disagreement remains unclear. It would greatly help our understanding of the nonlinear and non-Newtonian rheology of particulate media if such higher-order theories could be tackled analytically or semi-analytically to obtain closed-form constitutive relations – this forms the primary motivation of the present work.

In this paper, we derive closed-form analytical expressions for all components of the stress tensor as well as the collisional dissipation rate of steady USF for the whole range of densities by considering terms up to super-Burnett order (i.e. third order in shear rate and temperature anisotropy). To achieve the above goal, we follow the anisotropic version of Grad's moment method (Jenkins & Richman 1988) and solve the balance equation for the second-moment of velocity fluctuations semi-analytically for the USF of smooth inelastic hard disks. In addition, we generalize this method for the non-uniform shear state and derive an explicit constitutive relation for heat flux. Our primary focus is to decipher an analytical understanding of how all the transport coefficients (shear viscosity, pressure and first normal stress difference) depend on different control parameters (e.g. density, restitution coefficient, shear rate, etc.) when one goes beyond the 'linear' NS regime via Grad's moment equations. Our second goal is to check whether the resulting moment theory can yield quantitative predictions for normal stress differences and other transport coefficients for the whole range of densities and restitution coefficients (e.g. at small values of the restitution coefficient). Both goals are achieved successfully from our super-Burnett-order constitutive relations as demonstrated in § 4. Furthermore, the validation of the derived nonlinear constitutive relations, via a comparison with molecular dynamics simulations (§ 5), at different densities confirms the appropriateness of the Enskog kinetic equation to describe the dense shear flow of inelastic hard disks.

The rest of this paper is organized as follows. Section 2 provides a brief overview of the kinetic theory, the Grad-level (second or higher order in gradients) hydrodynamic equations and the anisotropic Gaussian distribution function. The construction of the second-moment tensor and its anisotropy in the USF, and the formulation of the second-moment equation in a rotated coordinate frame, are described in § 3. The collision integrals in the moment equations are approximated by an infinite series as outlined in § 4, followed by the explicit forms of resulting moment equations at Burnett and super-Burnett orders. An exact analytical solution for 'leading-order' moment equations is derived in § 4.1. The super-Burnett-order expressions for all components of the stress tensor, along with shear viscosity, pressure and first normal stress difference, are discussed in § 4.2. That the Grad-level dissipation rate depends on both the shear rate and the temperature anisotropy is discussed in § 4.3. The degenerate nature of the uniform shear state is discussed in § 4.4 in terms of its inherent 'non-Newtonian' rheology. The accuracy of our super-Burnett-order constitutive relations is verified in § 5.1 via a comparison with the full numerical solution. In addition to comparing with the molecular dynamics simulation data, § 5.2 establishes the superior predictions of the present moment theory with respect to an NS-order constitutive model (Lutsko 2005; Garzo, Santos & Montanero 2007). A comparative discussion of our results with another Grad-level theory (Kremer & Marques 2011; Garzo 2012) as well as with a Chapman–Enskog-based Burnett-order theory (Sela, Goldhirsch & Noskowicz 1996) for a dilute system is made in § 5.3. In § 6 we consider the non-uniform shear state and outline a procedure to derive the constitutive relation for the 'non-Fourier' heat flux. The conclusions are given in § 7.

2. Overview of Enskog kinetic theory and Grad-level moment equations

Let us consider a dense granular gas consisting of N randomly moving smooth inelastic hard disks of diameter σ and mass m. Let $\boldsymbol{c}_1$ and $\boldsymbol{c}_2$ be the velocities of two disks before a collision, with $\boldsymbol{c}_1'$ and $\boldsymbol{c}_2'$ being their post-collisional velocities, respectively. The collision dynamics for instantaneous and binary collisions is governed by

$$(\boldsymbol{g}' \cdot \boldsymbol{k}) = -e(\boldsymbol{g} \cdot \boldsymbol{k}), \tag{2.1}$$

where $\boldsymbol{g} \equiv \boldsymbol{g}_{12} = \boldsymbol{c}_1 - \boldsymbol{c}_2$ and $\boldsymbol{g}' = \boldsymbol{c}_1' - \boldsymbol{c}_2'$ are the pre- and post-collisional relative velocities, respectively, and $\boldsymbol{k} \equiv \boldsymbol{k}_{12} = (\boldsymbol{x}_2 - \boldsymbol{x}_1)/|\boldsymbol{x}_2 - \boldsymbol{x}_1|$ is the unit contact vector joining the centre of disk 1 to that of disk 2 at collision. In (2.1), e is the coefficient of normal restitution, with $e = 1$ and 0 referring to perfectly elastic and sticking collisions, respectively. Since the disks are assumed to be smooth, there is no change in their tangential component of relative velocity (i.e. $\boldsymbol{k} \times \boldsymbol{g}' = \boldsymbol{k} \times \boldsymbol{g}$).

At the mesoscopic level, this system is described by the Liouville equation for an N-particle distribution function, which can be reduced to an infinite hierarchy of evolution equations of distribution functions (one-body, two-body, three-body, etc.), known as the BBGKY (for Bogoliubov–Born–Green–Kirkwood–Yvon) hierarchy (Chapman & Cowling 1970). The first member of this hierarchy deals with the evolution of the single-particle distribution function $f(\boldsymbol{c}, \boldsymbol{x}, t)$, which, in the absence of any body force, reads

$$\left(\frac{\partial}{\partial t} + \boldsymbol{c} \cdot \boldsymbol{\nabla}\right) f = J(f^{(2)}), \tag{2.2}$$

where $\boldsymbol{\nabla}$ is the gradient operator in the configuration space and $J(f^{(2)})$ is the collision integral, which that depends on the two-particle distribution function $f^{(2)}(\boldsymbol{c}_1, \boldsymbol{x}_1, \boldsymbol{c}_2, \boldsymbol{x}_2, t)$. The transition from the mesoscopic to the macroscopic level is made via the hydrodynamic or coarse-grained fields, which are nothing but the moments of $f(\boldsymbol{c}, \boldsymbol{x}, t)$ of various orders. In addition to (i) the mass density

$$\rho(\boldsymbol{x}, t) \equiv m\, n(\boldsymbol{x}, t) = m \int f(\boldsymbol{c}, \boldsymbol{x}, t)\, \mathrm{d}\boldsymbol{c}, \tag{2.3}$$

where $n(\boldsymbol{x}, t) = N/V$ is the number density of particles, and (ii) the coarse-grained velocity

$$\boldsymbol{u}(\boldsymbol{x}, t) \equiv \langle \boldsymbol{c} \rangle = \frac{1}{n(\boldsymbol{x}, t)} \int \boldsymbol{c} f(\boldsymbol{c}, \boldsymbol{x}, t)\, \mathrm{d}\boldsymbol{c}, \tag{2.4}$$

we choose (iii) the full second-moment tensor

$$\boldsymbol{M}(\boldsymbol{x}, t) \equiv \langle \boldsymbol{C}\boldsymbol{C} \rangle = \frac{1}{n(\boldsymbol{x}, t)} \int \boldsymbol{C}\boldsymbol{C} f(\boldsymbol{c}, \boldsymbol{x}, t)\, \mathrm{d}\boldsymbol{c}, \tag{2.5}$$

where $\boldsymbol{C} \equiv \boldsymbol{c} - \boldsymbol{u}$ is the peculiar or fluctuation velocity of the particles, as a separate hydrodynamic field. The trace of (2.5) is the granular temperature

$$T(\boldsymbol{x}, t) \equiv \left\langle \frac{1}{2} \boldsymbol{C} \cdot \boldsymbol{C} \right\rangle = \frac{1}{2n(\boldsymbol{x}, t)} \int \boldsymbol{C}^2 f(\boldsymbol{c}, \boldsymbol{x}, t)\, \mathrm{d}\boldsymbol{c}, \tag{2.6}$$

which constitutes a hydrodynamic field at the NS order. Note that this definition of temperature (2.6) is commonly used in the granular mechanics community (Savage & Jeffrey 1981; Jenkins & Richman 1985*a*,*b*; Goldhirsch 2003; Rao & Nott 2008),

although the usual definition (Chapman & Cowling 1970) incorporating the mass m and the Boltzmann constant k_B has also been adopted by many (Brilliantov & Pöschel 2004; Santos *et al.* 2004; Lutsko 2005). In either case, it must be noted that the granular temperature is not a thermodynamic temperature (Goldhirsch 2003).

The evolution equations for hydrodynamic fields are obtained from the kinetic equation (2.2) by multiplying it by a particle property $\psi = \psi(\boldsymbol{c})$ and integrating it over the velocity space, resulting in the following master balance equation:

$$\frac{\partial}{\partial t}\langle n\psi\rangle = -\boldsymbol{\nabla}\cdot\langle n\boldsymbol{c}\psi\rangle + \mathfrak{C}[\psi]. \tag{2.7}$$

Here

$$\left.\begin{aligned}\mathfrak{C}[\psi] &= \iiint_{\boldsymbol{g}\cdot\boldsymbol{k}>\boldsymbol{0}} (\psi_2' - \psi_2) f^{(2)}(\boldsymbol{c}_1, \boldsymbol{x} - \sigma\boldsymbol{k}, \boldsymbol{c}_2, \boldsymbol{x}, t)\, \sigma\,(\boldsymbol{k}\cdot\boldsymbol{g})\, \mathrm{d}\boldsymbol{k}\, \mathrm{d}\boldsymbol{c}_1\, \mathrm{d}\boldsymbol{c}_2 \\ &= \iiint_{\boldsymbol{g}\cdot\boldsymbol{k}>\boldsymbol{0}} (\psi_1' - \psi_1) f^{(2)}(\boldsymbol{c}_1, \boldsymbol{x}, \boldsymbol{c}_2, \boldsymbol{x} + \sigma\boldsymbol{k}, t)\, \sigma\,(\boldsymbol{k}\cdot\boldsymbol{g})\, \mathrm{d}\boldsymbol{k}\, \mathrm{d}\boldsymbol{c}_1\, \mathrm{d}\boldsymbol{c}_2\end{aligned}\right\} \tag{2.8}$$

is the collisional rate of production of ψ per unit area, with $\boldsymbol{g}\cdot\boldsymbol{k} > 0$ referring to the constraint of impending collisions. It is straightforward to decompose (2.8) into the form (Jenkins & Richman 1985*a*,*b*; Rao & Nott 2008)

$$\mathfrak{C}[\psi] = \aleph[\psi] - \boldsymbol{\nabla}\cdot\boldsymbol{\Theta}[\psi] - \boldsymbol{\Theta}\left[\frac{\partial\psi}{\partial\boldsymbol{C}}\right] : \boldsymbol{\nabla}\boldsymbol{u}, \tag{2.9}$$

where $\boldsymbol{\Theta}[\psi]$ and $\aleph[\psi]$ are the collisional flux and production or source terms, respectively, whose integral expressions are given in §§ A.1 and A.2, respectively. Note that the origin of the collisional flux $\boldsymbol{\Theta}[\psi]$ is tied to the excluded volume of the 'macroscopic' particles and hence this term vanishes for a 'dilute' system of point particles. Combining (2.9) and (2.7), the master balance equation simplifies to (Jenkins & Richman 1985*a*,*b*, 1988)

$$\frac{\partial}{\partial t}\langle n\psi\rangle = -\left\langle n\left(\frac{\partial}{\partial t} + \boldsymbol{c}\cdot\boldsymbol{\nabla}\right) u_\alpha \frac{\partial\psi}{\partial C_\alpha}\right\rangle - \boldsymbol{\nabla}\cdot(\langle n\boldsymbol{c}\psi\rangle + \boldsymbol{\Theta}[\psi]) - \boldsymbol{\Theta}\left[\frac{\partial\psi}{\partial\boldsymbol{C}}\right] : \boldsymbol{\nabla}\boldsymbol{u} + \aleph[\psi]. \tag{2.10}$$

Substituting $\psi = 1$, c_α and $C_\alpha C_\beta$ into (2.10), we obtain the balance equations

$$\frac{\mathrm{D}\rho}{\mathrm{D}t} = -\rho u_{\alpha,\alpha}, \tag{2.11}$$

$$\rho\frac{\mathrm{D}u_\alpha}{\mathrm{D}t} = -P_{\alpha\beta,\alpha}, \tag{2.12}$$

$$\rho\frac{\mathrm{D}M_{\alpha\beta}}{\mathrm{D}t} = -Q_{\gamma\alpha\beta,\gamma} - P_{\delta\beta}u_{\alpha,\delta} - P_{\delta\alpha}u_{\beta,\delta} + \aleph_{\alpha\beta}, \tag{2.13}$$

for the mass, momentum and second moment, respectively. In the above, $\mathrm{D}/\mathrm{D}t = \partial/\partial t + u_\alpha(\partial/\partial x_\alpha)$ is the convective derivative, the subscript following a comma denotes a partial derivative (i.e. $u_{\alpha,\alpha} \equiv \partial u_\alpha/\partial x_\alpha$) with Einstein's summation convention over

repeated indices, and

$$P_{\alpha\beta} = \rho\langle \boldsymbol{C}_\alpha \boldsymbol{C}_\beta\rangle + \Theta_\alpha[mC_\beta] \equiv \rho M_{\alpha\beta} + \Theta_{\alpha\beta}, \tag{2.14}$$

$$Q_{\gamma\alpha\beta} = \rho\langle C_\gamma C_\alpha C_\beta\rangle + \Theta_\gamma[mC_\alpha C_\beta] \equiv \rho M_{\gamma\alpha\beta} + \Theta_{\gamma\alpha\beta}, \tag{2.15}$$

$$\aleph_{\alpha\beta} = \aleph[mC_\alpha C_\beta] \tag{2.16}$$

are the total stress tensor (momentum flux), the flux of the second moment, and the collisional source of the second moment (dissipation), respectively. In (2.14) and (2.15), the first term represents the kinetic contribution and the second term is its collisional contribution.

The trace of (2.13) yields the well-known balance equation for granular energy,

$$\rho\frac{\mathrm{D}T}{\mathrm{D}t} = -q_{\alpha,\alpha} - P_{\alpha\beta}u_{\beta,\alpha} - \mathscr{D}, \tag{2.17}$$

where

$$\mathscr{D} \equiv -\tfrac{1}{2}\aleph_{\beta\beta} = -\tfrac{1}{2}\aleph[mC^2] \tag{2.18}$$

is the rate of dissipation of energy per unit area (i.e. in two dimensions) and

$$q_\alpha \equiv \tfrac{1}{2}Q_{\alpha\beta\beta} = \tfrac{1}{2}\rho M_{\alpha\beta\beta} + \tfrac{1}{2}\Theta_{\alpha\beta\beta} \tag{2.19}$$

is the heat-flux vector. In (2.13), we assume that the deviatoric part of $Q_{\gamma\alpha\beta}$, i.e.

$$\widehat{Q}_{\gamma\alpha\beta} = Q_{\gamma\alpha\beta} - \tfrac{1}{4}(Q_{\gamma\xi\xi}\delta_{\alpha\beta} + Q_{\alpha\xi\xi}\delta_{\gamma\beta} + Q_{\beta\xi\xi}\delta_{\alpha\gamma}), \tag{2.20}$$

is zero, thus leaving only the contracted third moment $M_{\alpha\beta\beta} = \langle C_\alpha C_\beta C_\beta\rangle$ as the relevant hydrodynamic variable at third order.

In summary, the balance equations (2.11), (2.12) and (2.13), along with the constraint $\widehat{Q}_{\gamma\alpha\beta} = 0$, constitute the minimal Grad-level description of a fluidized granular matter in terms of moment equations that incorporates normal stress difference. The second-moment balance equation (2.13) can be replaced by its deviatoric part and the standard granular energy equation (2.17); the former equation is identically satisfied at the NS-level description. To close the balance equations (2.11)–(2.13), we need constitutive relations for the stress tensor (2.14), the collisional dissipation rate $\mathscr{D}$ (or the second-moment source term $\aleph_{\alpha\beta}$, (2.16)) and the heat flux (2.19). While the expressions for the first two constitutive quantities are derived for the uniform shear state as discussed in §§ 3 and 4, the heat flux requires a consideration of the non-uniform shear flow since the temperature gradient vanishes in the USF, which is dealt in § 6.

2.1. *Anisotropic Gaussian distribution function*

The constitutive relations require an evaluation of the collision integrals (see appendix A), which involve the two-particle distribution function. We adopt Boltzmann's *stosszahlansatz* (molecular chaos assumption) for which

$$f^{(2)}(\boldsymbol{c}_1, \boldsymbol{x} - \sigma\boldsymbol{k}, \boldsymbol{c}_2, \boldsymbol{x}, t) = g_0(\nu) f(\boldsymbol{c}_1, \boldsymbol{x} - \sigma\boldsymbol{k}, t) f(\boldsymbol{c}_2, \boldsymbol{x}, t). \tag{2.21}$$

Here $g_0(\nu)$ is the contact value of the radial distribution function whose functional form is taken to be (Verlet & Levesque 1982)

$$g_0(\nu) = \frac{(1 - 7\nu/16)}{(1-\nu)^2}, \tag{2.22}$$

with ν $(= n\pi\sigma^2/4)$ being the area fraction (density) of particles. As in the work of Jenkins & Richman (1988), we assume that the single-particle velocity distribution is an 'anisotropic' Gaussian

$$f(\boldsymbol{c}, \boldsymbol{x}, t) = \frac{n}{2\pi|\boldsymbol{M}|^{1/2}} \exp\left(-\frac{1}{2}\boldsymbol{C}\cdot\boldsymbol{M}^{-1}\cdot\boldsymbol{C}\right), \tag{2.23}$$

where $|\boldsymbol{M}| = \det(\boldsymbol{M})$ is the determinant of the second moment, which reduces to the standard Maxwellian or Gaussian distribution function for the case of isotropic $M_{\alpha\beta} = T\delta_{\alpha\beta}$. The ansatz of (2.23) as a solution for the homogeneous sheared system is tantamount to choosing an extended set of hydrodynamic fields, since the anisotropic Gaussian is a function of all components of the second moment, $\boldsymbol{M} = \langle \boldsymbol{CC}\rangle$, of the fluctuation velocity. Such an approach of choosing the generalized or anisotropic Gaussian as the reference state for a non-equilibrium system has been pioneered in the planetary physics community (Goldreich & Tremaine 1978; Shukhman 1984; Araki & Tremaine 1986; Schmidt *et al.* 2001; Latter & Ogilvie 2006) dealing with the modelling of Saturn's ring (Esposito 2006). This formalism has also been adopted by the granular matter community (Jenkins & Richman 1988; Chou & Richman 1998; Lutsko 2004) and can be applied to study the rheology of an arbitrary sheared state (as a perturbation of the homogeneous sheared system) via the well-known Hermite expansion (Lutsko 2004). This differs from Grad's original moment method (Grad 1949; Jenkins & Richman 1985*a*,*b*; Torrilhon & Struchtrup 2004; Vega Reyes, Santos & Garzo 2013) in which the reference state is a Gaussian representing the rest state of thermal equilibrium, and the deviations from the 'local' equilibrium are modelled via a Hermite expansion with unknown coefficients. In § 6, we will discuss an orthonormal expansion around (2.23) to derive the constitutive relation for the heat flux.

3. Steady uniform shear and the second-moment tensor

Let us focus on the two-dimensional coordinate system (since we are dealing with an assembly of disks) as depicted in figure 2, with x and y denoting the flow and gradient directions, respectively. The USF is described by the velocity-gradient tensor

$$\boldsymbol{\nabla u} = \begin{bmatrix} 0 & 2\dot{\gamma} \\ 0 & 0 \end{bmatrix} \equiv \boldsymbol{D} + \boldsymbol{W}, \tag{3.1}$$

such that the velocity field is $\boldsymbol{u} = (u, v) = (2\dot{\gamma}y, 0)$, where $2\dot{\gamma} = \mathrm{d}u/\mathrm{d}y$ is the uniform (constant) shear rate. The shear and spin tensors are given by

$$\boldsymbol{D} = \begin{bmatrix} 0 & \dot{\gamma} \\ \dot{\gamma} & 0 \end{bmatrix} \quad \text{and} \quad \boldsymbol{W} = \begin{bmatrix} 0 & \dot{\gamma} \\ -\dot{\gamma} & 0 \end{bmatrix}. \tag{3.2a,b}$$

The eigenvalues of $\boldsymbol{D}$ are $\pm\dot{\gamma}$ with respective eigenvectors

$$|D_1\rangle = \begin{bmatrix} \cos\frac{1}{4}\pi \\ \sin\frac{1}{4}\pi \end{bmatrix} \quad \text{and} \quad |D_2\rangle = \begin{bmatrix} -\sin\frac{1}{4}\pi \\ \cos\frac{1}{4}\pi \end{bmatrix}. \tag{3.3a,b}$$

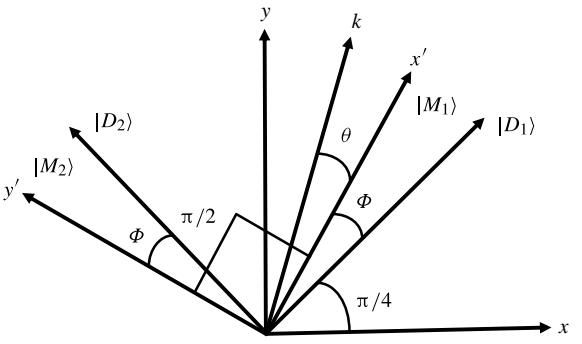

FIGURE 2. A sketch of the coordinate frame: $|D_1\rangle$ and $|D_2\rangle$ are the eigen-directions of the shear tensor $\boldsymbol{D}$, and $|M_1\rangle$ and $|M_2\rangle$ are the eigen-directions of the second-moment tensor $\boldsymbol{M}$.

These eigen-directions are sketched in figure 2. To formulate the anisotropic moment theory for the USF in two dimensions, we follow the work of Jenkins & Richman (1988) in §§ 3.1 and 3.2. Next we simplify our analysis of the second-moment balance by working in a rotated coordinate frame as discussed in § 3.3.

3.1. *Anisotropy in the second-moment tensor*

Here we analyse the second-moment tensor $\boldsymbol{M}$ in terms of its eigenvalues and eigenvectors. Let M_1 and M_2 be the eigenvalues of $\boldsymbol{M}$, with associated eigenvectors $|M_1\rangle$ and $|M_2\rangle$, respectively. We assume that the eigenvector $|M_1\rangle$ makes an angle ϕ with the eigenvector $|D_1\rangle$ of the shear tensor $\boldsymbol{D}$ (see (3.3)). Since $|M_1\rangle$ and $|M_2\rangle$ are orthogonal, the eigenvector $|M_2\rangle$ makes the same angle ϕ with $|D_2\rangle$; this is illustrated in figure 2. The expression for the second-moment tensor $\boldsymbol{M}$ is

$$\begin{aligned}\boldsymbol{M} &= M_1 \begin{bmatrix}\cos(\phi+\frac{1}{4}\pi)\\ \sin(\phi+\frac{1}{4}\pi)\end{bmatrix}\begin{bmatrix}\cos(\phi+\frac{1}{4}\pi) & \sin(\phi+\frac{1}{4}\pi)\end{bmatrix}\\ &\quad + M_2 \begin{bmatrix}-\sin(\phi+\frac{1}{4}\pi)\\ \cos(\phi+\frac{1}{4}\pi)\end{bmatrix}\begin{bmatrix}-\sin(\phi+\frac{1}{4}\pi) & \cos(\phi+\frac{1}{4}\pi)\end{bmatrix}\\ &\equiv T\begin{bmatrix}1+\eta\sin 2\phi & -\eta\cos 2\phi\\ -\eta\cos 2\phi & 1-\eta\sin 2\phi\end{bmatrix} = T[\delta_{\alpha\beta}] + \widehat{\boldsymbol{M}},\end{aligned} \tag{3.4}$$

where we have defined the following variables:

$$2T \equiv M_{\alpha\alpha} = M_1 + M_2, \tag{3.5}$$

$$\eta \equiv (M_2 - M_1)/2T, \tag{3.6}$$

and $\widehat{\boldsymbol{M}}$ is the deviatoric part of the second moment,

$$\widehat{\boldsymbol{M}} = \eta T\begin{bmatrix}\sin 2\phi & -\cos 2\phi\\ -\cos 2\phi & -\sin 2\phi\end{bmatrix}. \tag{3.7}$$

It is clear from (3.4) that the diagonal elements of $\boldsymbol{M}$ are not equal, and η is a measure of the anisotropy of the second-moment tensor. Moreover, the angle ϕ (see figure 2)

measures the rotation that makes $\boldsymbol{M}$ diagonal (see § 3.3). It is straightforward to verify that

$$|\boldsymbol{M}| = T^2(1-\eta^2), \tag{3.8}$$

$$M_1 = T(1-\eta) \quad \text{and} \quad M_2 = T(1+\eta), \tag{3.9a,b}$$

with $M_2 > M_1$.

Let us introduce the 'Savage–Jeffrey' number (Savage & Jeffrey 1981)

$$R = \frac{\sigma\dot{\gamma}}{4\sqrt{T}} \equiv \frac{\dot{\gamma}}{4\sqrt{T/\sigma^2}}, \tag{3.10}$$

which can be interpreted as the scaled or dimensionless shear rate and also as the inverse of the square root of the dimensionless temperature. It is evident from (3.4) and (3.10) that R, η and ϕ are three unknown parameters that completely characterize the anisotropic second-moment tensor $\boldsymbol{M}$ in USF. Recall that the stress tensor (2.14) is $\boldsymbol{P} \equiv \rho\boldsymbol{M}$ in the dilute limit. Hence the anisotropy of $\boldsymbol{M}$ is responsible for the first normal stress difference ($P_{xx} - P_{yy} \sim \eta \sin 2\phi$) in the dilute limit, which is one signature of the stress tensor being non-Newtonian.

3.2. *The second-moment balance equation in uniform shear flow*

For the steady USF, the number density n, velocity gradient $\boldsymbol{\nabla u}$, granular temperature T and the components of $\boldsymbol{M}$ are constant, and therefore the mass and momentum balance equations are identically satisfied. The balance equation for the second-moment tensor (2.13) reduces to

$$P_{\delta\beta}u_{\alpha,\delta} + P_{\delta\alpha}u_{\beta,\delta} = \aleph_{\alpha\beta}, \tag{3.11}$$

where

$$P_{\alpha\beta} = \rho M_{\alpha\beta} + \Theta_{\alpha\beta} \tag{3.12}$$

is the total stress tensor. The kinetic stress $\rho M_{\alpha\beta}$ is calculated from (3.4), and the collisional stress can be written as (see § A.1)

$$\Theta_{\alpha\beta} = \frac{2(1+e)\rho\nu g_0(\nu)}{\pi^{3/2}} \int k_\alpha k_\beta (\boldsymbol{k}\cdot\boldsymbol{M}\cdot\boldsymbol{k})\mathfrak{G}(\chi)\,\mathrm{d}\boldsymbol{k}. \tag{3.13}$$

The collisional source of second moment $\aleph_{\alpha\beta}$ in (3.11) can be decomposed as (Jenkins & Richman 1988)

$$\aleph_{\alpha\beta} = A_{\alpha\beta} + \widehat{B}_{\alpha\beta} = A_{\alpha\beta} + \widehat{E}_{\alpha\beta} + \widehat{G}_{\alpha\beta} + \Theta_{\alpha\gamma}W_{\beta\gamma} + \Theta_{\beta\gamma}W_{\alpha\gamma}, \tag{3.14}$$

where

$$A_{\alpha\beta} = -\frac{4(1-e^2)\rho\nu g_0(\nu)}{\sigma\,\pi^{3/2}} \int k_\alpha k_\beta (\boldsymbol{k}\cdot\boldsymbol{M}\cdot\boldsymbol{k})^{3/2}\mathfrak{F}(\chi)\,\mathrm{d}\boldsymbol{k}, \tag{3.15}$$

and $\widehat{B}_{\alpha\beta}$, $\widehat{E}_{\alpha\beta}$ and $\widehat{G}_{\alpha\beta}$ represent traceless tensors, which also possess similar integral expressions as detailed in § A.2. The contact vector $\boldsymbol{k}$ over which the above integrations have to be performed and its unit normal $\boldsymbol{j}$ can be expressed as

$$\boldsymbol{k} = \begin{bmatrix} \cos(\theta+\phi+\frac{1}{4}\pi) \\ \sin(\theta+\phi+\frac{1}{4}\pi) \end{bmatrix} \quad \text{and} \quad \boldsymbol{j} = \begin{bmatrix} \sin(\theta+\phi+\frac{1}{4}\pi) \\ -\cos(\theta+\phi+\frac{1}{4}\pi) \end{bmatrix}. \tag{3.16a,b}$$

We have assumed that θ is the angle between $\boldsymbol{k}$ and $|M_1\rangle$ (the eigenvector corresponding to the smaller eigenvalue of $\boldsymbol{M}$, (3.9)) as illustrated in figure 2. It is straightforward to verify that

$$\boldsymbol{k}\cdot\boldsymbol{M}\cdot\boldsymbol{k}\equiv T+\boldsymbol{k}\cdot\widehat{\boldsymbol{M}}\cdot\boldsymbol{k}=T(1-\eta\cos 2\theta)\quad\text{and}\quad\boldsymbol{j}\cdot\boldsymbol{M}\cdot\boldsymbol{k}=-T\eta\sin 2\theta. \tag{3.17a,b}$$

In (3.13) and (3.15) and related collision integrals, the integrands are expressed in terms of two analytic functions $\mathfrak{F}(\chi)$ and $\mathfrak{G}(\chi)$ defined as (Araki & Tremaine 1986; Jenkins & Richman 1988):

$$\mathfrak{F}(\chi)\equiv-\sqrt{\pi}(\tfrac{3}{2}\chi+\chi^3)\operatorname{erfc}(\chi)+(1+\chi^2)\exp(-\chi^2), \tag{3.18}$$

$$\mathfrak{G}(\chi)\equiv\sqrt{\pi}(\tfrac{1}{2}+\chi^2)\operatorname{erfc}(\chi)-\chi\exp(-\chi^2), \tag{3.19}$$

where

$$\chi=\frac{\sigma(\boldsymbol{k}\cdot\boldsymbol{\nabla u}\cdot\boldsymbol{k})}{2\sqrt{\boldsymbol{k}\cdot\boldsymbol{M}\cdot\boldsymbol{k}}}=\frac{2R\cos 2(\theta+\phi)}{(1-\eta\cos 2\theta)^{1/2}}\equiv\chi(\eta,R,\phi,\theta). \tag{3.20}$$

It is clear from (3.16), (3.17) and (3.20) that the integrations over $\boldsymbol{k}$ in (3.13)–(3.15) are to be carried out over θ via $\mathrm{d}\boldsymbol{k}=\mathrm{d}\theta$, with $\theta\in(0,2\pi)$. It is worth pointing out that $\chi=0$ in the dilute limit, since the origin of this term is tied to the excluded-volume effects of macroscopic particles.

With the aid of (3.12) and (3.14), the balance of second moment (3.11) finally reduces to

$$\rho M_{\delta\beta}(D_{\alpha\delta}+W_{\alpha\delta})+\Theta_{\delta\beta}D_{\alpha\delta}+\rho M_{\delta\alpha}(D_{\beta\delta}+W_{\beta\delta})+\Theta_{\delta\alpha}D_{\beta\delta}=A_{\alpha\beta}+\widehat{E}_{\alpha\beta}+\widehat{G}_{\alpha\beta}. \tag{3.21}$$

This is the central equation that must be solved to obtain the rheological quantities (shear viscosity, pressure and first normal stress difference) of USF for the whole range of densities ν. Furthermore, the Grad-level collisional dissipation rate is calculated from (3.14).

3.3. *Reduced second-moment equations in rotated coordinate frame*

Equation (3.21) is significantly simplified if $\boldsymbol{M}$ is made diagonal. This is achieved by using

$$\mathscr{R}=\begin{bmatrix}\cos(\phi+\frac{1}{4}\pi) & -\sin(\phi+\frac{1}{4}\pi)\\ \sin(\phi+\frac{1}{4}\pi) & \cos(\phi+\frac{1}{4}\pi)\end{bmatrix} \tag{3.22}$$

as the rotation matrix with respect to the coordinate frame $x'y'$, with x' and y' being directed along $|M_1\rangle$ and $|M_2\rangle$, respectively (see figure 2). In the rotated $x'y'$ frame, the second-moment tensor is diagonal,

$$\boldsymbol{M}'=T\begin{bmatrix}1-\eta & 0\\ 0 & 1+\eta\end{bmatrix}, \tag{3.23}$$

with the prime indicating that the quantity is evaluated in this new frame, and

$$\boldsymbol{k}' = \begin{bmatrix} \cos\theta \\ \sin\theta \end{bmatrix}, \quad \boldsymbol{j}' = \begin{bmatrix} \sin\theta \\ -\cos\theta \end{bmatrix}, \tag{3.24a,b}$$

$$\boldsymbol{u}' = 2\dot{\gamma}[x' \sin(\phi + \tfrac{1}{4}\pi) + y' \cos(\phi + \tfrac{1}{4}\pi)] \begin{bmatrix} \cos(\phi + \frac{1}{4}\pi) \\ -\sin(\phi + \frac{1}{4}\pi) \end{bmatrix}, \tag{3.25}$$

and

$$\boldsymbol{D}' = \dot{\gamma} \begin{bmatrix} \cos 2\phi & -\sin 2\phi \\ -\sin 2\phi & -\cos 2\phi \end{bmatrix}, \quad \boldsymbol{W}' = \dot{\gamma} \begin{bmatrix} 0 & 1 \\ -1 & 0 \end{bmatrix}. \tag{3.26a,b}$$

It is clear from (3.23) that the anisotropy of $\boldsymbol{M}$ is characterized solely by the temperature difference η as defined in (3.6). Note that the non-zero component of vorticity is in the direction orthogonal to the plane of the motion, and hence the spin tensor is invariant under the planar rotation (3.22).

In the rotated coordinate frame, the components of (3.21) are its trace

$$-2\eta\rho T\dot{\gamma} \cos 2\phi + \dot{\gamma}(\Theta_{x'x'} - \Theta_{y'y'}) \cos 2\phi - 2\dot{\gamma}\Theta_{x'y'} \sin 2\phi = \tfrac{1}{2}(A_{x'x'} + A_{y'y'}), \tag{3.27}$$

the deviatoric component

$$2\rho T\dot{\gamma} \cos 2\phi + \dot{\gamma}(\Theta_{x'x'} + \Theta_{y'y'}) \cos 2\phi = \tfrac{1}{2}(A_{x'x'} - A_{y'y'}) + \widehat{E}_{x'x'} + \widehat{G}_{x'x'}, \tag{3.28}$$

and the off-diagonal component

$$2\rho T\dot{\gamma}(\eta - \sin 2\phi) - \dot{\gamma}(\Theta_{x'x'} + \Theta_{y'y'}) \sin 2\phi = A_{x'y'} + \widehat{E}_{x'y'} + \widehat{G}_{x'y'}. \tag{3.29}$$

The integral terms appearing in (3.27)–(3.29) can be expressed as

$$\left.\begin{aligned}
A_{x'x'} + A_{y'y'} &= \frac{-4\rho\nu g_0(1-e^2)T^{3/2}}{\sigma\pi^{3/2}} \mathscr{H}_{003}(\eta, R, \phi), \\
A_{x'x'} - A_{y'y'} &= \frac{-4\rho\nu g_0(1-e^2)T^{3/2}}{\sigma\pi^{3/2}} \mathscr{H}_{103}(\eta, R, \phi), \\
A_{x'y'} &= \frac{-2\rho\nu g_0(1-e^2)T^{3/2}}{\sigma\pi^{3/2}} \mathscr{H}_{013}(\eta, R, \phi), \\
\widehat{E}_{x'x'} &= \frac{4\rho\nu g_0(1+e)T^{3/2}\eta}{\sigma\pi^{3/2}} \mathscr{H}_{021}(\eta, R, \phi), \\
\widehat{E}_{x'y'} &= -\frac{4\rho\nu g_0(1+e)T^{3/2}\eta}{\sigma\pi^{3/2}} \mathscr{H}_{111}(\eta, R, \phi),
\end{aligned}\right\} \tag{3.30}$$

$$\left.\begin{aligned}
\widehat{G}_{x'x'} &= \frac{2\rho\nu g_0(1+e)T\dot{\gamma}}{\pi^{3/2}} [\cos 2\phi\, \mathscr{J}_{020}(\eta, R, \phi) \\
&\quad + \sin 2\phi\, \mathscr{J}_{110}(\eta, R, \phi) - \eta \sin 2\phi\, \mathscr{J}_{010}(\eta, R, \phi)], \\
\widehat{G}_{x'y'} &= -\frac{2\rho\nu g_0(1+e)T\dot{\gamma}}{\pi^{3/2}} [\cos 2\phi\, \mathscr{J}_{110}(\eta, R, \phi) \\
&\quad + \sin 2\phi\, \mathscr{J}_{200}(\eta, R, \phi) - \eta \sin 2\phi\, \mathscr{J}_{100}(\eta, R, \phi)], \\
\Theta_{x'x'} + \Theta_{y'y'} &= \frac{2\rho\nu g_0(1+e)T}{\pi^{3/2}} \mathscr{J}_{002}(\eta, R, \phi), \\
\Theta_{x'x'} - \Theta_{y'y'} &= \frac{2\rho\nu g_0(1+e)T}{\pi^{3/2}} \mathscr{J}_{102}(\eta, R, \phi), \\
\Theta_{x'y'} &= \frac{\rho\nu g_0(1+e)T}{\pi^{3/2}} \mathscr{J}_{012}(\eta, R, \phi).
\end{aligned}\right\} \tag{3.31}$$

Here $\mathscr{H}_{\alpha\beta\gamma}$ and $\mathscr{J}_{\alpha\beta\gamma}$ possess the integral expressions

$$\mathscr{H}_{\alpha\beta\gamma}(\eta, R, \phi) \equiv \int_0^{2\pi} \cos^{\alpha} 2\theta \sin^{\beta} 2\theta\, (1-\eta\cos 2\theta)^{\gamma/2} \mathfrak{F}(\chi[\eta, R, \phi, \theta])\, \mathrm{d}\theta, \quad (3.32)$$

$$\mathscr{J}_{\alpha\beta\gamma}(\eta, R, \phi) \equiv \int_0^{2\pi} \cos^{\alpha} 2\theta \sin^{\beta} 2\theta\, (1-\eta\cos 2\theta)^{\gamma/2} \mathfrak{G}(\chi[\eta, R, \phi, \theta])\, \mathrm{d}\theta, \quad (3.33)$$

with $\mathfrak{F}(\chi)$ and $\mathfrak{G}(\chi)$ given by (3.18) and (3.19).

Equations (3.27)–(3.29) represent a system of nonlinear integro-algebraic equations, which we solve using two different methods: (i) semi-analytical method and (ii) numerical method. In § 4 we outline a semi-analytical series solution (which reduces to the solution of Jenkins & Richman (1988) in the dense limit) and verify *a posteriori*, via a comparison with the full numerical solution (see § 5.1), that the adopted power-series representation of integrals (3.32) and (3.33) holds for the whole range of densities. More importantly, this helps to achieve our primary goal of deriving closed-form analytical expressions for nonlinear transport coefficients as well as for the dissipation rate that are valid from dilute to dense flows as we show in §§ 4.2 and 4.3, respectively.

4. Non-Newtonian stress tensor and dissipation rate: constitutive relations

The solution of (3.27)–(3.29) involves evaluating the integrals in (3.32) and (3.33) whose integrands are functions of $\mathfrak{F}(\chi)$ and $\mathfrak{G}(\chi)$ as defined in (3.18) and (3.19), respectively, with χ being given by (3.20). Using the power-series representation for the complementary error function and the exponential, the two functions $\mathfrak{F}(\chi)$ and $\mathfrak{G}(\chi)$ can be compactly expressed as

$$\begin{aligned}\mathfrak{F}(\eta, R, \phi, \theta) \;=\; & -\sqrt{\pi}\left[\frac{3}{2}\frac{2R\cos(2\phi+2\theta)}{(1-\eta\cos 2\theta)^{1/2}} + \left(\frac{2R\cos(2\phi+2\theta)}{(1-\eta\cos 2\theta)^{1/2}}\right)^3\right] \\ & + \sum_{m=0}^{\infty} \frac{(-1)^m}{m!}\frac{3}{(2m-1)(2m-3)}\left[\frac{2R\cos(2\phi+2\theta)}{(1-\eta\cos 2\theta)^{1/2}}\right]^{2m}, \quad (4.1)\end{aligned}$$

$$\begin{aligned}\mathfrak{G}(\eta, R, \phi, \theta) \;=\; & \sqrt{\pi}\left[\frac{1}{2} + \frac{4R^2\cos^2(2\phi+2\theta)}{(1-\eta\cos 2\theta)}\right] \\ & + \sum_{m=0}^{\infty} \frac{(-1)^m}{m!}\frac{2}{4m^2-1}\left[\frac{2R\cos(2\phi+2\theta)}{(1-\eta\cos 2\theta)^{1/2}}\right]^{2m+1}. \quad (4.2)\end{aligned}$$

Substituting (4.1) and (4.2) into (3.32) and (3.33) and carrying out term-by-term integrations over $\theta \in (0, 2\pi)$ results in an infinite series in η and R for each integral in (3.32) and (3.33) (see appendix B). To progress further, we need to truncate each series after a finite number of terms.

Retaining terms up to second order in η and R (i.e. $O(\eta^2)$, $O(\eta R)$ and $O(R^2)$) in the integral expressions for $\mathscr{H}_{\alpha\beta\gamma}$ ((3.32) and (B 6) in appendix B) and for $\mathscr{J}_{\alpha\beta\gamma}$ ((3.33)

and (B 7) and (B 8) in appendix B), (3.27)–(3.29) simplify to

$$\left.\begin{aligned}
&4\pi^{3/2}\eta R\cos 2\phi+(1+e)\nu g_0 R(16\pi R+2\pi^{3/2}\eta\cos 2\phi)\\
&\quad=\nu g_0(1-e^2)(3\pi^{3/2}\eta R\cos 2\phi+2\pi+\tfrac{3}{8}\pi\eta^2+12\pi R^2),\\
&4\pi^{3/2}R\cos 2\phi-(1+e)\nu g_0(2\pi\eta-\tfrac{1}{16}\pi\eta^3-2\pi^{3/2}R\cos 2\phi-12\pi^{3/2}R^3\cos 2\phi\\
&\qquad-4\pi\eta R^2+8\pi\eta R^2\sin^2 2\phi)\\
&\quad=\nu g_0(1-e^2)[3\pi^{3/2}R\cos 2\phi+\tfrac{3}{2}\pi\eta],\\
&4\pi^{3/2}R(\eta-\sin 2\phi)-(1+e)\nu g_0 R(2\pi^{3/2}\sin 2\phi+12\pi^{3/2}R^2\sin 2\phi+4\pi\eta R\sin 4\phi)\\
&\quad=-3\pi^{3/2}\nu g_0(1-e^2)R\sin 2\phi.
\end{aligned}\right\}\tag{4.3}$$

At the third order in η and R (i.e. up to $O(\eta^3)$, $O(\eta^2R)$, $O(\eta R^2)$ and $O(R^3)$) they are

$$\left.\begin{aligned}
&4\pi^{3/2}\eta R\cos 2\phi+(1+e)\nu g_0 R(16\pi R+16\pi R^3+2\pi^{3/2}\eta\cos 2\phi-\tfrac{1}{2}\pi\eta^2 R\\
&\qquad-\pi R\eta^2\cos^2 2\phi)\\
&\quad=\nu g_0(1-e^2)(3\pi^{3/2}\eta R\cos 2\phi+2\pi+\tfrac{3}{8}\pi\eta^2+12\pi R^2),\\
&4\pi^{3/2}R\cos 2\phi-(1+e)\nu g_0(2\pi\eta-\tfrac{1}{16}\pi\eta^3-2\pi^{3/2}R\cos 2\phi-12\pi^{3/2}R^3\cos 2\phi\\
&\qquad+8\pi\eta R^2\sin^2 2\phi-4\pi R^2\eta)\\
&\quad=\nu g_0(1-e^2)[3R\pi^{3/2}\cos 2\phi+6\pi^{3/2}R^3\cos 2\phi+\tfrac{3}{2}\pi\eta+\tfrac{3}{2}\pi\eta R^2(2+\cos 4\phi)],\\
&4\pi^{3/2}R(\eta-\sin 2\phi)-(1+e)\nu g_0 R\left(2\pi^{3/2}\sin 2\phi+12\pi^{3/2}R^2\sin 2\phi+4\pi\eta R\sin 4\phi\right)\\
&\quad=-\nu g_0(1-e^2)(3\pi^{3/2}R\sin 2\phi+6\pi^{3/2}R^3\sin 2\phi+\tfrac{3}{2}\pi\eta R^2\sin 4\phi).
\end{aligned}\right\}\tag{4.4}$$

It is clear that we have three unknowns η, R and ϕ to solve for at each order, provided the restitution coefficient e and the area fraction ν are specified. Both sets of coupled algebraic equations, (4.3) and (4.4), can be easily solved using the Newton–Raphson method.

Equations (4.3) and (4.4) can be thought of as analogues of the Burnett-order (quadratic in shear rate) and super-Burnett-order (cubic in shear rate) equations, respectively, and this will become evident in § 4.1, where we show that $\eta\sim O(R)$ to leading order. In principle we can retain further higher-order terms to solve the above three equations but stop at the cubic order as they provide adequate accuracy to recover the exact numerical solution, as we shall demonstrate in § 5.1.

4.1. *Exact solution at leading order: scaling relations*

Before moving to numerical solution of (4.3) and (4.4), it is illuminating to consider the leading-order moment equations that admit an exact solution, which helps to understand the scaling relations for the three unknowns η, R and ϕ in terms of the restitution coefficient e. Retaining only the zeroth-order terms in η and R in the integral expressions for $\mathscr{H}_{\alpha\beta\gamma}$ and $\mathscr{J}_{\alpha\beta\gamma}$ (see (B 6)–(B 8) in appendix B), the following equations for the second-moment balance are obtained:

$$\left.\begin{aligned}
2\sqrt{\pi}\eta R\cos 2\phi-(1-e^2)\nu g_0=0,\\
2\sqrt{\pi}R\cos 2\phi-(1+e)\nu g_0\eta+\sqrt{\pi}(1+e)\nu g_0 R\cos 2\phi=0,\\
2(\eta-\sin 2\phi)-(1+e)\nu g_0\sin 2\phi=0.
\end{aligned}\right\}\tag{4.5}$$

These equations are amenable to analytical solution, and yield

$$\left.\begin{aligned} \eta &= \sqrt{(1-e)(1+\tfrac{1}{2}(1+e)\nu g_0)} \sim (1-e)^{1/2}, \\ R &= \frac{\sqrt{(1-e^2)(1+e)}\,\nu g_0}{\sqrt{2\pi(2e+(1+e)\nu g_0)}} \sim (1-e)^{1/2}, \\ \sin 2\phi &= \sqrt{\frac{2(1-e)}{2+(1+e)\nu g_0}} \sim (1-e)^{1/2}, \\ \cos 2\phi &= \sqrt{\frac{2e+(1+e)\nu g_0}{2+(1+e)\nu g_0}}, \\ \frac{\eta}{R} &= \frac{\sqrt{\pi(2+(1+e)\nu g_0)(2e+(1+e)\nu g_0)}}{(1+e)\nu g_0}, \end{aligned}\right\} \tag{4.6}$$

with each quantity being a function of e and ν only. Note further that

$$\frac{\eta}{R}\cos 2\phi = \sqrt{\pi}\left(1+\frac{2e}{(1+e)\nu g_0}\right). \tag{4.7}$$

It is clear from (4.6) that the temperature anisotropy η, the shear rate R and $\sin 2\phi$ scale as $\epsilon \equiv (1-e)^{1/2}$ (a measure of the inelasticity of particle collisions). More importantly, that both η and R are of the same order lends credence to the adopted power-series expansion of the collision integrals (3.32) and (3.33) in terms of η and R (see appendix B). The leading-order scaling of R and η with ϵ implies that the NS-, Burnett- and super-Burnett-order terms in the USF are of order $O(\epsilon)$, $O(\epsilon^2)$ and $O(\epsilon^3)$, respectively, although we have not attempted to establish this connection at higher orders (see the discussion in § 4.4). In the rest of this paper, the second- and third-order terms in R and η are referred to as Burnett and super-Burnett order, respectively.

4.2. *Non-Newtonian stress tensor: analytical expressions for transport coefficients*

The dimensionless stress tensor can be written as

$$\boldsymbol{P}^* = \frac{\boldsymbol{P}}{\rho_p U_R^2} = \begin{pmatrix} P^*_{xx} & P^*_{xy} \\ P^*_{yx} & P^*_{yy} \end{pmatrix} \equiv \begin{pmatrix} p^* & 0 \\ 0 & p^* \end{pmatrix} - \begin{pmatrix} -\mathscr{N}^*_{1/2} & \mu^* \\ \mu^* & \mathscr{N}^*_{1/2} \end{pmatrix}, \tag{4.8}$$

where $p^* = (P^*_{xx}+P^*_{yy})/2$ is the pressure, $\mu^* = -P^*_{xy}$ is the shear viscosity and $\mathscr{N}_1^* = P^*_{xx}-P^*_{yy}$ is the first normal stress difference. Here ρ_p is the material (intrinsic) density of particles and $U_R = 2\dot{\gamma}\sigma$ is the reference velocity scale. We will express constitutive relations in terms of the dimensionless temperature, which is defined as

$$T^* = \frac{T}{U_R^2} \equiv \frac{1}{64R^2}. \tag{4.9}$$

The power series (4.2) for $\mathfrak{G}(\eta, R, \phi)$ is inserted into (3.13) to evaluate the collisional stress, and the total stress tensor is subsequently obtained from (3.12). In the following we present only the final analytical expressions for the components of the stress tensor, thus leaving the related algebraic details to appendix C.

4.2.1. *Shear viscosity: up to super-Burnett order*

Retaining terms up to the third order in temperature anisotropy η and shear rate R, the dimensionless shear stress takes the following form (see appendix C):

$$\frac{P^*_{xy}}{\nu T^*} = -\eta\cos 2\phi - \frac{4\nu g_0(1+e)}{\sqrt{\pi}}\left[R\left(1+\frac{\sqrt{\pi}}{8}\frac{\eta}{R}\cos 2\phi\right) + \underbrace{R^3\left(1-\frac{\eta^2}{32R^2}(1+2\cos^2 2\phi)\right)}\right] + O(\eta^m R^n, m+n\geqslant 4). \tag{4.10}$$

The first term on the right-hand side represents its kinetic contribution and the remaining part its collisional contribution. Recall from (4.7) that $(\eta/R)\cos 2\phi \sim O(1)$, and hence the underbraced terms in (4.10) are of super-Burnett ($O(R^3)$) order.

The expression for the dimensionless shear viscosity, $\mu^* = \mu/\rho_p\sigma U_R \equiv -P_{xy}/\rho_p U_R^2 = -P^*_{xy}$, follows from (4.10):

$$\mu^* = \frac{\nu\sqrt{T^*}}{8}\left[\frac{\eta}{R}\cos 2\phi + \frac{4\nu g_0(1+e)}{\sqrt{\pi}}\left(1+\frac{\sqrt{\pi}}{8}\frac{\eta}{R}\cos 2\phi + \underbrace{R^2-\frac{\eta^2}{32}(1+2\cos^2 2\phi)}\right)\right] + O(\eta^m R^n, m+n\geqslant 4). \tag{4.11}$$

The nonlinear dependence of viscosity on the shear rate R and the temperature anisotropy η is evident from the underbraced terms in (4.11).

For a check, we consider the NS-order shear viscosity

$$\mu^* = \frac{\nu\sqrt{T^*}}{8}\left[\frac{\eta}{R}\cos 2\phi + \frac{4\nu g_0(1+e)}{\sqrt{\pi}}\left(1+\frac{\sqrt{\pi}}{8}\frac{\eta}{R}\cos 2\phi\right)\right] + O(R^2), \tag{4.12}$$

which follows from (4.11) by neglecting the nonlinear terms. Substituting the leading-order solution (4.7) into (4.12), we obtain the expressions for the kinetic and collisional parts of the shear viscosity as

$$\mu^*_k \equiv \frac{\nu\sqrt{T^*}}{8}\left(\frac{\eta}{R}\cos 2\phi\right) = \frac{\nu\sqrt{T^*}}{8}\sqrt{\pi}\left(1+\frac{2e}{(1+e)\nu g_0}\right), \tag{4.13}$$

$$\mu^*_c = \frac{\nu^2 g_0(1+e)\sqrt{T^*}}{2\sqrt{\pi}}\left[1+\frac{\pi}{8}\left(1+\frac{2e}{(1+e)\nu g_0}\right)\right], \tag{4.14}$$

respectively, at NS order. These expressions (4.13) and (4.14) with $e=1$ agree perfectly with the known results for the shear viscosity (Jenkins & Richman 1985*a*) of an elastic hard-disk system.

4.2.2. *Pressure: up to super-Burnett order*

At the third-order approximation in η and R, the diagonal components of the stress tensor are

$$\frac{P^*_{xx}}{\nu T^*} = (1+\eta\sin 2\phi) + \nu g_0(1+e)\left(1+\frac{1}{2}\eta\sin 2\phi + 4R^2 + \frac{2}{\sqrt{\pi}}\eta R\cos 2\phi - \frac{1}{4\sqrt{\pi}}R\eta^2\sin 2\phi\cos 2\phi\right) + O(\eta^m R^n, m+n\geqslant 4), \tag{4.15}$$

$$\frac{P_{yy}^*}{\nu T^*} = (1-\eta\sin 2\phi) + \nu g_0(1+e)\left(1-\frac{1}{2}\eta\sin 2\phi + 4R^2 + \frac{2}{\sqrt{\pi}}\eta R\cos 2\phi + \frac{1}{4\sqrt{\pi}}R\eta^2\sin 2\phi\cos 2\phi\right) + O(\eta^m R^n, m+n\geqslant 4). \tag{4.16}$$

Note that both contain odd-order terms in η and R having opposite signs, and hence they cancel each other, resulting in the following expression for the mean pressure:

$$p^* = \nu T^*\left[1+\nu g_0(1+e)\left(1+\underbrace{4R^2+\frac{2}{\sqrt{\pi}}\eta R\cos 2\phi}\right)\right] + O(\eta^m R^n, m+n\geqslant 4). \tag{4.17}$$

This expression holds at both second and third order of approximation in η and R. In any case, it is clear that the collisional part of the pressure depends on the shear rate R and the temperature anisotropy η, revealing the nonlinear dependence of pressure at the Burnett order $O(R^2)$ and beyond. Neglecting the 'underbraced' terms in (4.17), we arrive at the textbook expression for pressure,

$$p^* = \nu T^*(1+\nu g_0(1+e)), \tag{4.18}$$

which holds at NS order.

4.2.3. *First normal stress difference*

Subtracting (4.16) from (4.15), we obtain an expression for the first normal stress difference:

$$P_{xx}^* - P_{yy}^* = 2\eta\sin(2\phi)\nu T^* + \nu^2 g_0(1+e)T^*\left(\eta\sin 2\phi - \frac{1}{2\sqrt{\pi}}R\eta^2\sin 2\phi\cos 2\phi\right) + \text{h.o.t.} \tag{4.19}$$

The leading term in (4.19) is of order $O(R^2)$, since $\eta\sin 2\phi = O(1-e) = O(R^2)$ following (4.6), and the terms of order $O(R)$ in (4.15) and (4.16) do not contribute to the normal stress difference. The leading correction in (4.19) comes from the collisional part of the stress tensor,

$$R\eta^2\sin 2\phi\cos 2\phi \equiv R^2(\eta\sin 2\phi)\left(\frac{\eta}{R}\cos 2\phi\right) = O(R^4), \tag{4.20}$$

which is fourth order in the shear rate.

Retaining terms up to $O(R^4)$ in (4.19), the scaled first normal stress difference is given by

$$\mathscr{N}_1 = \frac{P_{xx}-P_{yy}}{p} = \frac{\eta\sin 2\phi\left(2+\nu g_0(1+e)\left(1-\frac{1}{2\sqrt{\pi}}R\eta\cos 2\phi\right)\right)}{1+\nu g_0(1+e)\left(1+4R^2+\frac{2}{\sqrt{\pi}}\eta R\cos 2\phi\right)}, \tag{4.21}$$

which is a measure of the normal stress with respect to the mean/isotropic pressure (4.17). Focusing on the dilute limit ($\nu\to 0$), (4.21) becomes

$$\mathscr{N}_1 = 2\eta\sin 2\phi = 2(1-e)\sim R^2\sim\dot{\gamma}^2, \tag{4.22}$$

which scales quadratically with the shear rate. This confirms that the normal stress difference is a Burnett-order effect (Sela & Goldhirsch 1998). Note from (4.21) that $\mathscr{N}_1 \sim \eta \sin 2\phi$ at any density and it approaches zero for $\eta \to 0$ and/or $\phi \to 0$. The origin of the normal stress difference is, therefore, tied to (i) the temperature anisotropy η and (ii) the angle ϕ between the eigen-directions of the shear tensor $\boldsymbol{D}$ and the second-moment tensor $\boldsymbol{M}$ – both are shear-induced effects.

It should be noted that the elastic limit ($e \to 1$) remains non-singular even though the temperature diverges ($T \sim R^{-2} \to \infty$ as $e \to 1$). The latter divergence is due to the absence of any mechanism to compensate the shear work, but this can be fixed by using a thermostat. Therefore, the normal stress difference is finite for perfectly elastic collisions (Sela *et al.* 1996; Alam & Luding 2003*a*,*b*):

$$\mathscr{N}_1 = 0.679 \frac{\dot{\gamma}^2 l_f^2}{T}, \tag{4.23}$$

where l_f is the mean free path. Note, however, that $\mathscr{N}_1 \sim O(10^{-20})$ in a sheared molecular gas at standard temperature and pressure with $\dot{\gamma} = O(1)$ and hence is negligible. The expression (4.23) can be understood from (4.22) by tying the in-built mechanism of energy replenishment in a granular gas with a thermostat in its molecular counterpart.

4.3. *Dissipation rate: dependence on shear rate and normal stress*

Employing the series solution for integrals, the collisional dissipation rate in the energy balance equation can be calculated from (3.14) as

$$\begin{aligned}
\mathscr{D} &\equiv -\frac{1}{2}\aleph_{\beta\beta} = -\frac{1}{2}(A_{\beta\beta} + \widehat{B}_{\beta\beta}) = -\frac{1}{2}(A_{x'x'} + A_{y'y'}) \\
&= \frac{2\rho\nu g_0(1-e^2)T^{3/2}}{\sigma\,\pi^{3/2}}\mathscr{H}_{003}(\eta, R, \phi) \\
&= \frac{4\rho\nu g_0(1-e^2)T^{3/2}}{\sigma\sqrt{\pi}}\left(1 + 6R^2\left(1 + \frac{\sqrt{\pi}}{4}\frac{\eta}{R}\cos 2\phi\right) + \frac{3}{16}\eta^2 + \text{h.o.t.}\right).
\end{aligned} \tag{4.24}$$

The neglected terms in (4.24) are of order $O(\eta^m R^n)$ with $m+n \geqslant 4$: the leading-order corrections are second order in both R and η but the odd-order terms ($m+n=1,3,\ldots$) are zero. Hence the expression (4.24) is exact up to the super-Burnett order. In the isotropic limit of zero normal stress difference ($\eta \to 0$ and $\phi \to 0$), (4.24) reduces to

$$\mathscr{D} = \mathscr{D}^{(0)}(1 + 6R^2 + O(R^4)), \tag{4.25}$$

which contains a rate-dependent correction term at the leading order. The origin of this correction is tied to the excluded-volume effects (3.20) of a dense gas. In (4.25),

$$\mathscr{D}^{(0)} = \frac{4\rho_p \nu^2 g_0(1-e^2)T^{3/2}}{\sigma\sqrt{\pi}} \tag{4.26}$$

is the dissipation rate for a system of inelastic hard disks (Jenkins & Richman 1985*a*), which holds at both Euler and NS orders. Equation (4.26), however, differs

from related NS-order theories (Lutsko 2005; Garzo *et al.* 2007) that are built around the homogeneous cooling state as a reference.

Returning to (4.24), we note that the correction terms beyond the NS order depend quadratically on both (i) the shear rate ($\dot{\gamma} \sim R \sim \epsilon \equiv (1-e)^{1/2}$) and (ii) the temperature anisotropy η ($\sim \epsilon$). The latter finding uncovers a novel dependence of the collisional dissipation rate on the normal stress difference since $\eta \sim \mathscr{N}_1$. As clarified in § 4.1, the above quadratic-order corrections in (4.24) can also be translated into an effective correction of $O(\epsilon^2)$, which agrees qualitatively with the related Burnett-order expression for $\mathscr{D}$ derived by Sela & Goldhirsch (1998) and Brilliantov & Pöschel (2003), who used the Chapman–Enskog method to solve the Boltzmann equation in three dimensions up to the Burnett order (i.e. the second order in the gradients of hydrodynamic fields). Note that the latter work analysed the homogeneous cooling state of a granular gas of viscoelastic particles by incorporating the second-order gradient terms in the two-particle distribution function.

4.4. *Inherent non-Newtonian rheology of uniform shear flow*

Let us now remark on the dependence of various transport coefficients on (i) the shear rate R, (ii) the temperature anisotropy η, (iii) the non-coaxiality angle ϕ, (iv) the restitution coefficient e and (v) the density or area fraction ν that we uncovered in §§ 4.2 and 4.3. It is clear from (4.6) that there is an intertwined relationship among R, η and ϕ via their dependence on e and ν in the uniform shear state, and this survives at any order. For example, (4.4) can be solved perturbatively by using (4.6) as the zeroth-order solution, leading to an approximate solution for η, R and ϕ as a function of $\epsilon = (1-e)^{1/2}$ for the whole range of densities. Substituting these values into (4.11) results in an expression for the shear viscosity as a function of e and ν. This implies that specifying ν and e with Lees–Edward boundary condition (Alam & Luding 2003*a*,*b*, 2005*a*,*b*; Gayen & Alam 2008) sets the granular temperature and the shear rate simultaneously, which is a consequence of the 'in-built' thermostat of collisional dissipation that balances the shear work. Therefore, it would not be possible to isolate the shear-rate dependence of viscosity (and other transport coefficients) from its dependence on inelasticity if we were to measure shear viscosity from the molecular dynamics simulation (§ 5.2) of a granular fluid under uniform shear.

What is measured in simulations is nothing but the non-Newtonian viscosity, since the shear rate is always finite, and hence the rheology of the uniform shear state of a granular fluid is inherently non-Newtonian (Santos *et al.* 2004) unlike in its elastic counterpart. The comparisons of transport coefficients in § 5.2 will validate their dependence on the density and the restitution coefficient at any arbitrary shear rate. On the other hand, the explicit rate dependence of transport coefficients can be checked in future with simulations of boundary-driven shear (with imposed temperature gradient) where the shear rate and the restitution coefficient can be independently varied (Vega Reyes *et al.* 2013).

5. Validation of constitutive relations and comparison with particle simulation

5.1. *Validation of constitutive relations: are super-Burnett terms required?*

Here we validate the constitutive relations for all transport coefficients as detailed in § 4.2. This is done by carrying out a comparison between the transport coefficients obtained from (i) the full numerical solution of moment equations and (ii) those obtained from their analytical expressions at Burnett (i.e. quadratic order in R and η) and super-Burnett (i.e. cubic order in R and η) orders. The goal is to check whether

we need to go beyond the Burnett order for an accurate representation of transport coefficients at any restitution coefficient for the whole range of densities.

For the complete numerical solution of the moment equations, we evaluate the integrals in $\boldsymbol{A}$, $\widehat{\boldsymbol{E}}$, $\widehat{\boldsymbol{G}}$ and Θ in (3.27)–(3.29) using the standard quadrature rule. Next we solve the resulting system of three nonlinear algebraic equations by the Newton–Raphson method, yielding values of η, R and ϕ for specified values of the area fraction ν and the restitution coefficient e. This helps to determine (see appendix C) the pressure p, the shear viscosity μ and the first normal stress difference $\mathscr{N}_1$ as functions of ν and e.

The comparison between the full moment theory and the series solutions at second and third orders is given in figure 3: panels (*a*)–(*d*), respectively, display the variations of pressure, shear viscosity, granular temperature and first normal stress difference with area fraction, for four values of the restitution coefficient ($e = 0.99$, 0.9, 0.6 and 0.3). In each panel, the continuous (black) and dashed (red online) lines represent the series solution at third- and second-order approximation, respectively, and the symbols denote the exact solution (full numerical solution) of the moment equations. We observe excellent agreement between the third-order series solution and the exact solution even at a strong dissipation of $e = 0.3$. In contrast, the second-order series solution does well only up to $e = 0.6$ for the normal stress difference (see panel (*d*)), although the pressure, viscosity and temperature are well predicted by the second-order solution even at $e = 0.3$.

On the whole, figure 3 confirms that, while the Burnett-order expressions yield accurate transport coefficients in the dilute limit, the super-Burnett-order terms are required to reproduce the correct behaviour of all transport coefficients at higher densities ($\nu > 0.2$) for the whole range of restitution coefficients ($0 \leqslant e \leqslant 1$).

To see why the adopted series expansion (4.1) and (4.2) works well, we plot the variations of η, R and ϕ in figure 4(*a–c*), respectively. Again, we observe excellent agreement between the exact solution (symbols) and the third-order series solution (solid line) for the whole range of densities up to a restitution coefficient of $e = 0.3$. However, the second-order solution (dashed line) for η in panel (*a*) is seen to deviate significantly from its exact solution at $e = 0.6$ beyond a moderate density of $\nu \sim 0.35$, and this disagreement occurs at a much lower density ($\nu \sim 0.2$) for $e = 0.3$. It is clear that both R and η are small in the dilute and dense limits, respectively, but they tend to become of order one in opposite limits. Nevertheless, the series representation (4.1) and (4.2) and the resulting power-series expansion of integrals (3.32) and (3.33) in terms of η and R (appendix B) works excellently for the whole range of densities even at strong dissipations, as illustrated in figure 4, if we retain the third-order terms as in (4.4).

5.2. *Comparison of anisotropic moment theory with simulation and Navier–Stokes model*

In this section we make a detailed comparison for all transport coefficients of the non-Newtonian stress tensor as obtained in § 4.2 from the moment theory with (i) particle simulations and (ii) an NS order model. The NS-order transport coefficients are taken from those of Lutsko (2005) as detailed in appendix D. Note that Lutsko's model holds for both disks and spheres; Garzo *et al.* (2007) also derived NS-level transport coefficients in arbitrary dimension using a modified Sonine expansion, and confirmed that the viscosity, pressure and dissipation rate are hardly affected in both approaches. It may be noted that both works carry out a Chapman–Enskog expansion around

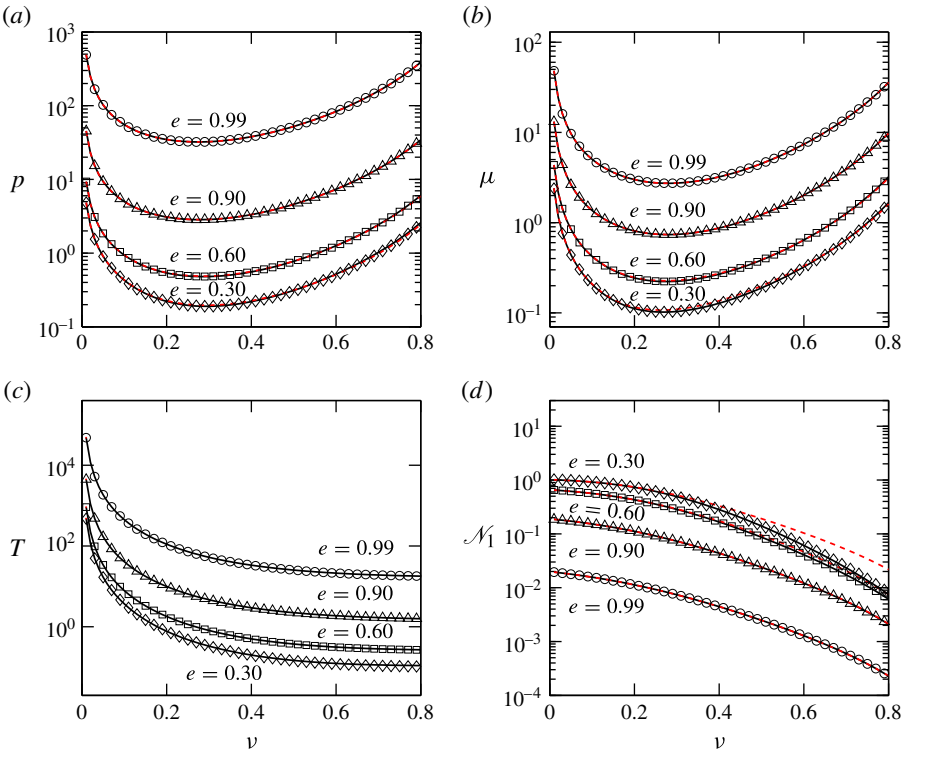

FIGURE 3. (Colour online) Comparison of the numerical solution for the moment theory (symbols) with approximate series solution: second-order (red dashed lines) and third-order (black solid line) series solutions for the (*a*) pressure, (*b*) shear viscosity, (*c*) granular temperature and (*d*) first normal stress difference.

the homogeneous cooling state, and the NS-level transport coefficients thus obtained are assumed to hold for all values of the restitution coefficient, since they made no assumption about the smallness of inelasticity or dissipation.

The event-driven simulation of the USF of inelastic hard disks (i.e. in two dimensions) has been carried out by Alam & Luding (2003*a*,*b*) and we take their data to compare with the present theory. The disks interact via the standard binary collision rule of smooth particles, (2.1), for a specified value of the restitution coefficient. The state of uniform shear is achieved by employing the Lees–Edward boundary condition (Lees & Edwards 1972). All simulations have been carried out in a square box with $N = 1024$ disks for two values of the restitution coefficient, $e = 0.9$ and 0.7, for a range of densities (area fractions) $\nu \in (0.01, 0.8)$ spanning from the dilute to the dense regime.

Figure 5 shows a comparison for the pressure field between (i) the exact moment theory (solid line, numerical solution), (ii) the NS-order model (dashed line) and (iii) simulation data (symbols). Panels (*a*)–(*c*), respectively, correspond to the total pressure ($p = p_k + p_c$), and its kinetic (p_k) and collisional (p_c) components; the data for $e = 0.9$ and 0.7 are marked in each panel. The analogue of figure 5 for the shear viscosity is displayed in figure 6. For both pressure and viscosity, we observe that the NS model overpredicts the simulation data, and the degree of discrepancy increases

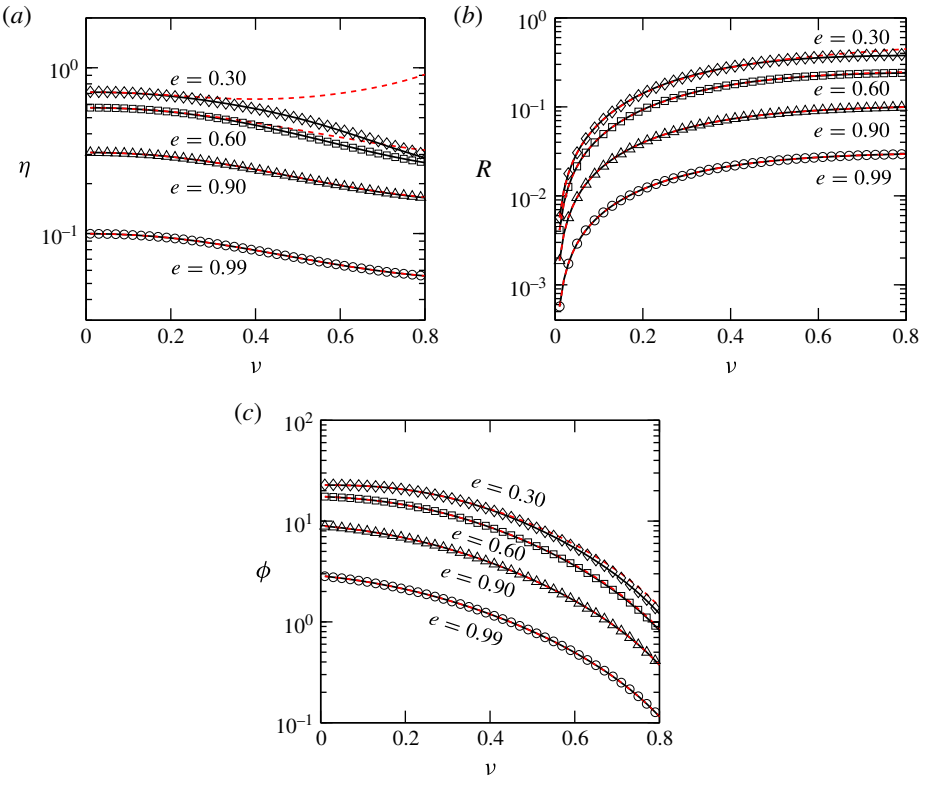

FIGURE 4. (Colour online) Comparison between the 'exact' (numerical solution) moment theory and the approximate series solution for a range of densities: variations of (*a*) η, (*b*) R and (*c*) ϕ (degrees) with area fraction. The symbols, dashed (red) and solid (black) lines represent the full numerical solution, second-order and third-order series solutions, respectively.

with decreasing value of e (i.e. with increasing dissipation). It is noteworthy that the deviation between the NS model and the simulation is more prominent for dilute flows at any restitution coefficient. In contrast, the predictions of the moment theory agree excellently with simulation even at $e = 0.7$ for a large range of densities – up to $\nu \sim 0.65$, which is close to the freezing point density $\nu_f \approx 0.69$ (see figures 5 and 6). A possible reason for quantitative discrepancies at large densities could be the breakdown of the molecular chaos assumption (§ 2.1), especially beyond the freezing density (Mitarai & Nakanishi 2007).

Figures 7 and 8 show the variations of the scaled pressure p/T and the scaled viscosity $\mu/\sqrt{T}$, respectively. In each figure, panels (*a*) and (*b*) correspond to $e = 0.9$ and 0.7, respectively, with the solid line, dashed line and symbols denoting the moment theory, NS theory and simulation data, respectively. Recall that both these scaled quantities ($p/T = f_1(\nu, e, \ldots)$ and $\mu/\sqrt{T} = f_2(\nu, e, \ldots)$) are functions solely of the density and restitution coefficient in the NS-level theory; however, they have additional dependence on the shear rate ($\dot{\gamma} \sim R$) as well as on the normal stress difference ($\mathscr{N}_1 \sim \eta$). Figure 7 indicates that the dependence of f_1 on R and η is negligible in dilute to moderately dense flows even at $e = 0.7$, but a slight deviation

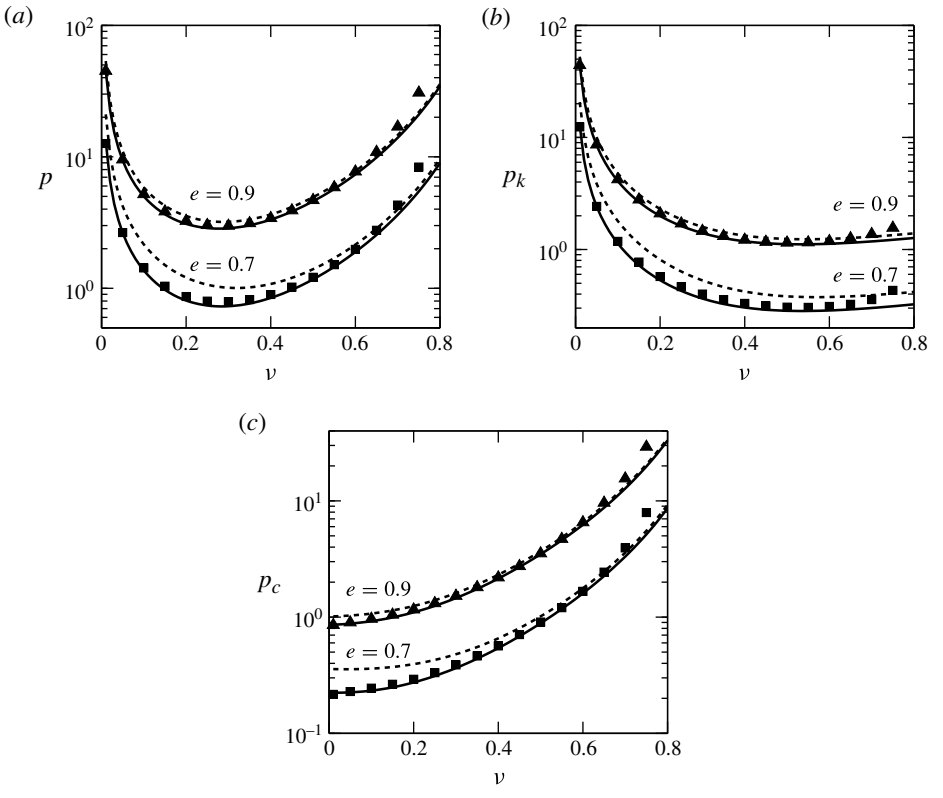

FIGURE 5. Comparison among the full moment theory (solid line, present work), the NS model (dashed line, Lutsko 2005) and simulation data (symbols) for the variation of pressure with area fraction: (*a*) total pressure $p = p_k + p_c$, (*b*) kinetic pressure p_k and (*c*) collisional pressure p_c. Results for two values of the restitution coefficient ($e = 0.9$ and 0.7) are shown.

(between the moment theory and the NS-level theory) is noticeable in the dense limit, which becomes more prominent with increasing dissipation. On the other hand, the viscosity function f_2 deviates strongly from its NS prediction in the dilute limit even at $e = 0.9$.

Figure 9 shows the variation of the scaled first normal stress difference $\mathscr{N}_1 = (P_{xx} - P_{yy})/p$ with density for three values of $e = 0.95$, 0.9 and 0.7. The lines correspond to the moment theory and the symbols to simulation data. Recall that $\mathscr{N}_1 = 0$ for all NS-order constitutive models. The prediction of the moment theory agrees well with simulation data for $e = 0.95$ and 0.9, but there are quantitative differences between theory and simulation that increase with increasing dissipation. Although the theoretical prediction remains good in the dilute limit ($\nu \to 0$) even at $e = 0.7$ (see also § 5.3 and figure 10), increasing the density leads to an underprediction of simulation data – this might be related to enhanced density correlations at finite densities. The latter assertion is supported by additional simulations at $e = 0.5$ (with other simulation parameters being fixed at finite densities) that show the emergence of particle clusters spanning over the whole system. Another noteworthy point in figure 9 is that the theory predicts $\mathscr{N}_1 \to 0$ in the dense limit, but

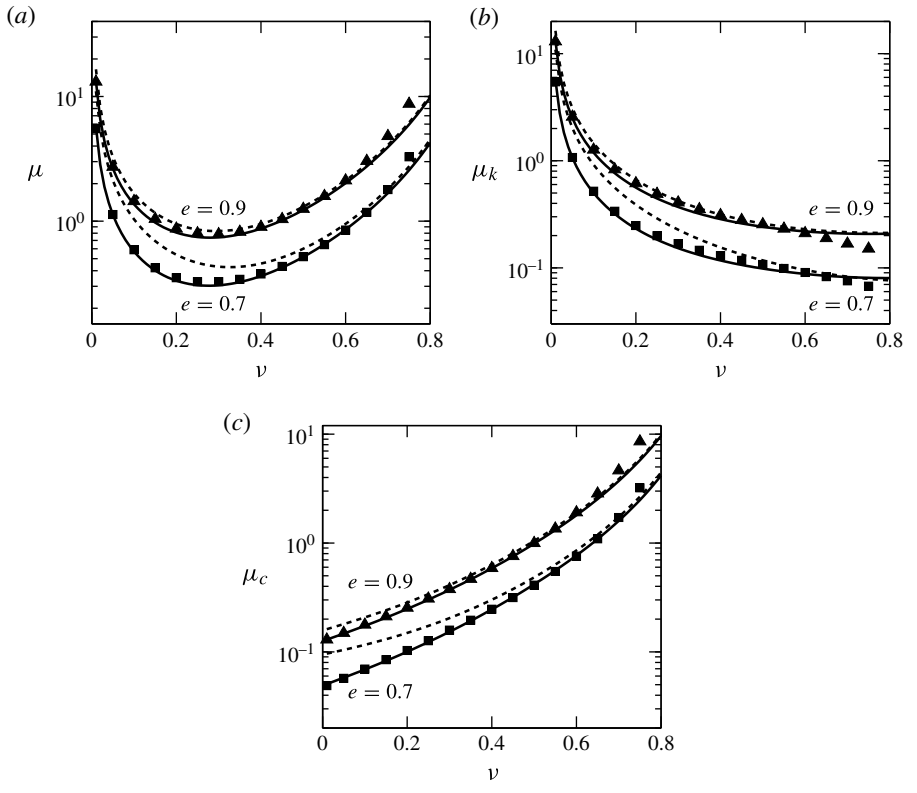

FIGURE 6. Same as figure 5 but for the variation of shear viscosity with area fraction: (*a*) total viscosity $\mu = \mu_k + \mu_c$, (*b*) kinetic viscosity μ_k and (*c*) collisional viscosity μ_c.

the simulation shows a sign reversal of $\mathscr{N}_1$ at some critical density (near the freezing density). This sign reversal of $\mathscr{N}_1$ is, in fact, tied to changes in the microstructure (Alam & Luding 2003*a*,*b*), i.e. changes in the pair correlation function and its relaxation under shear. The latter effect is not incorporated in the present theory, which is likely to be responsible for the disagreement between theory and simulation in the dense regime.

On the whole, we find that the Grad-level moment theory with anisotropic Gaussian can quantitatively predict the pressure and shear viscosity for a range of densities up to the freezing point at very strong dissipations ($e = 0.3$). In contrast the NS model (Lutsko 2005; Garzo *et al.* 2007), which is assumed to hold at any dissipation, shows quantitative discrepancies even at moderate dissipations ($e = 0.9$) and the degree of disagreement increases with decreasing restitution coefficient e. Last but not least, the missing ingredient of any NS-order constitutive model, the normal stress difference ($\mathscr{N}_1$, figure 9), is well predicted by our anisotropic moment theory, although quantitative discrepancy remains at finite densities for large dissipations.

5.3. *Comparison with another Grad-level theory in the dilute limit*

In this section we compare our analytical transport coefficients (§ 4.2) with those derived from another variant of Grad's method (Kremer & Marques 2011; Garzo 2012). In the latter two works, the moment theory was developed using a Hermite

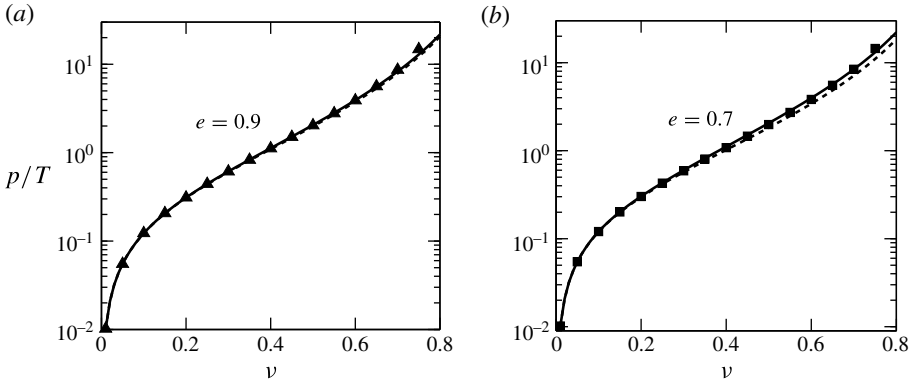

FIGURE 7. Variation of p/T (dimensionless) with area fraction for (*a*) $e = 0.9$ and (*b*) $e = 0.7$. The solid and dashed lines represent the exact moment theory (i.e. the full numerical solution) and the NS-order model (Lutsko 2005), respectively, and the symbols denote simulation data.

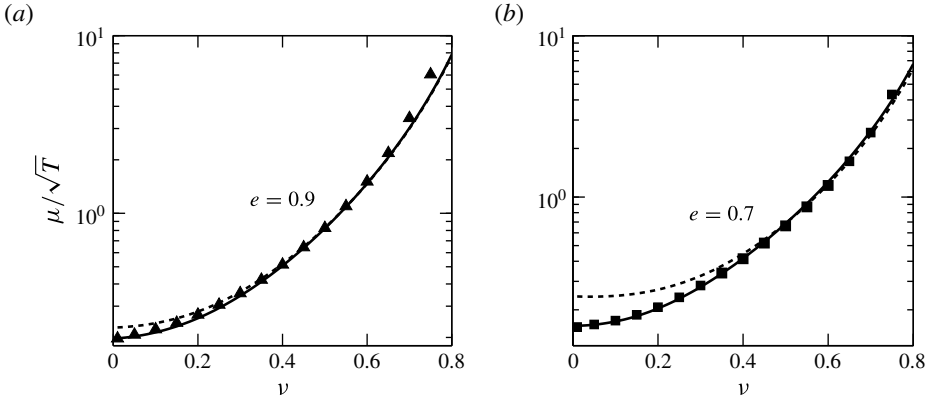

FIGURE 8. Variation of $\mu/\sqrt{T}$ (dimensionless) with area fraction for (*a*) $e = 0.9$ and (*b*) $e = 0.7$. The solid and dashed lines represent the exact moment theory (i.e. the full numerical solution) and the NS-order model (Lutsko 2005), respectively, and the symbols denote simulation data.

expansion around an isotropic Gaussian state, in contrast to the anisotropic Gaussian reference in our work. Leaving aside the mathematical details, we note that the balance equation for the second moment in the steady uniform shear state is the same as (3.11) as elaborated in § 3.2. An approximate expression for the source term has been determined for hard disks (Garzo 2012):

$$\aleph_{\alpha\beta} = -\varphi_\mu \widehat{P}_{\alpha\beta} - \zeta p \delta_{\alpha\beta}, \tag{5.1}$$

where $\widehat{P}_{\alpha\beta} = P_{\alpha\beta} - p\delta_{\alpha\beta}$ is the pressure deviator. The equation of state is $p \equiv (P_{xx} + P_{yy})/2 = \rho T$, and the expressions for the cooling rate ζ, collision frequency φ_μ (related to shear viscosity) and the coefficient of the fourth velocity cumulant α_2 $(= \langle C^4 \rangle / \langle C^4 \rangle^{(0)} - 1$, with the superscript '0' denoting its evaluation for a Gaussian or

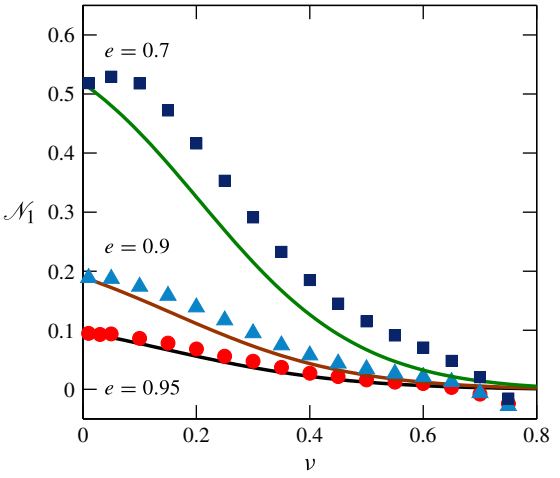

FIGURE 9. (Colour online) Variation of the scaled first normal stress difference $\mathscr{N}_1$ with area fraction. The symbols and lines represent the molecular dynamics simulation data and the present moment theory, respectively.

Maxwellian) are given by

$$\left.\begin{aligned} \zeta &= \frac{4\nu}{\sigma\sqrt{\pi}}(1-e^2)\left(1+\frac{3\alpha_2}{16}\right)\sqrt{T}, \\ \varphi_\mu &= \frac{\nu}{\sigma\sqrt{\pi}}(7-3e)(1+e)\left(1-\frac{\alpha_2}{32}\right)\sqrt{T}, \\ \alpha_2 &\equiv \left(\frac{\langle C^4\rangle}{\langle C^4\rangle^{(0)}}-1\right) = \frac{16(1-e)(1-2e^2)}{57-25e+30(1-e)e^2}. \end{aligned}\right\} \tag{5.2}$$

Note that $\alpha_2 = 0$ for a Maxwellian distribution function.

With the aid of (5.1) and taking the overall shear rate in the USF as $\mathrm{d}u/\mathrm{d}y = 2\dot{\gamma}$ (defined in (3.1)), (3.11) can be decomposed into its component forms:

$$\left.\begin{aligned} \varphi_\mu P_{xy} &= -2\dot{\gamma}P_{yy}, \\ (\varphi_\mu-\zeta)P_{xx} &= (\varphi_\mu+\zeta)P_{yy}, \\ 8\dot{\gamma}P_{xy} &= -(\varphi_\mu+\zeta)P_{xx}+(\varphi_\mu-\zeta)P_{yy}. \end{aligned}\right\} \tag{5.3}$$

The solution of (5.3) yields the diagonal components of the stress tensor,

$$\frac{P_{xx}}{4\rho_p\dot{\gamma}^2\sigma^2} = \frac{\nu}{64R^2}\left(\frac{\varphi_\mu+\zeta}{\varphi_\mu}\right) \quad \text{and} \quad \frac{P_{yy}}{4\rho_p\dot{\gamma}^2\sigma^2} = \frac{\nu}{64R^2}\left(\frac{\varphi_\mu-\zeta}{\varphi_\mu}\right), \tag{5.4a,b}$$

and the dimensionless shear rate R is

$$R^2 = \frac{\dot{\gamma}^2\sigma^2}{16T} = \frac{\nu^2(7-3e)^2(1+e)^2(1-e)(1-\frac{1}{32}\alpha_2)^2(1+\frac{3}{16}\alpha_2)}{16\pi(3+e-\frac{1}{32}\alpha_2(31-27e))}. \tag{5.5}$$

The expression for the first normal stress difference is

$$\mathscr{N}_1 = \frac{2(P_{xx}-P_{yy})}{(P_{xx}+P_{yy})} = \frac{2\zeta}{\varphi_\mu} = \frac{8(1-e)(1+\frac{3}{16}\alpha_2)}{(7-3e)(1-\frac{1}{32}\alpha_2)} \sim (1-e) \sim R^2, \tag{5.6}$$

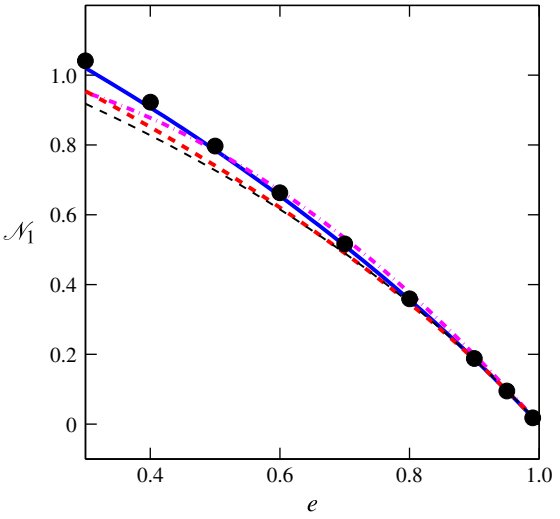

FIGURE 10. (Colour online) Comparison of the first normal stress difference obtained from simulation (symbols) with the present anisotropic Gaussian theory (blue solid line), the Grad-level theory of Garzo (thick red dashed line, (5.6)) and the Burnett-order theory of Sela & Goldhirsch (magenta dot-dashed line). The 'thin' black dashed line corresponds to (5.6) with $\alpha_2 = 0$ (see the text in § 5.3 for details). The area fraction is set to $\nu = 0.01$.

which scales quadratically with the shear rate and hence is a Burnett-order effect as confirmed in § 4.2.3.

The comparison of (5.6) with the present theory and the particle simulation data is shown in figure 10, marked by the red dashed line, the blue solid line and the circles, respectively; the simulations were carried out for an average area fraction of $\nu = 0.01$. The Burnett-order expression of Sela *et al.* (1996), obtained from the Chapman–Enskog expansion, is also displayed on the same figure (magenta dot-dashed line). We observe that the simulation data agree uniformly with the present anisotropic Gaussian theory for a large range of restitution coefficients $e \in (0.3, 0.99)$, but the Grad-level expression (5.6) of Garzo underpredicts the simulation results for $e < 0.8$. On the other hand, the Burnett theory of Sela *et al.* agrees well with simulation and present theory up to $e = 0.5$ and underpredicts $\mathscr{N}_1$ for $e < 0.5$. To ascertain the relative importance of the fourth velocity cumulant α_2 for a quantitative prediction of $\mathscr{N}_1$, we set $\alpha_2 = 0$ in (5.6) and plot the resulting expression as the 'thin' black dashed line in figure 10. It is clear that the fourth velocity cumulant does not affect $\mathscr{N}_1$ noticeably up to a restitution coefficient of $e \approx 0.6$ but underpredicts it slightly for smaller e.

From (5.3) and (5.4), the expressions for shear viscosity $\mu = -P_{xy}/2\dot{\gamma}$ and pressure $p = (P_{xx} + P_{yy})/2$ can be obtained as

$$\frac{\mu}{2\rho_p \dot{\gamma}\sigma^2} = \frac{\nu^2(1-e^2)(1+\frac{3}{16}\alpha_2)}{128\sqrt{\pi}R^3} \quad \text{and} \quad \frac{p}{4\rho_p \dot{\gamma}^2\sigma^2} = \frac{\nu}{64R^2}, \tag{5.7a,b}$$

with R being given by (5.5). These two expressions (5.7) are compared in figure 11, denoted by the red dashed lines, with (i) the particle simulation (denoted by symbols) and (ii) the present anisotropic Gaussian theory (blue solid lines). The curves for two variants of the NS-level theory (Lutsko 2005, green dot-dashed lines;

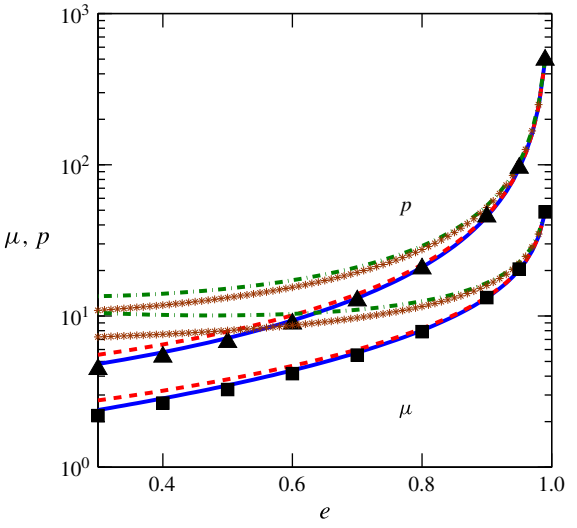

FIGURE 11. (Colour online) Comparison for dimensionless pressure and shear viscosity obtained from molecular dynamics simulation (symbols) with the present anisotropic Gaussian theory (blue solid lines), the Grad-level theory of Garzo (red dashed lines, (5.7)), the NS-level theory of Lutsko (2005, green dot-dashed lines) and the NS-level theory of Jenkins & Richman (1985*a*, magenta starred lines). Other parameters are as in figure 10.

and Jenkins & Richman 1985*a*, magenta starred lines) are also displayed. We see excellent agreement of simulation data with the present theory, but the isotropic version of the moment theory slightly overpredicts both p and μ for $e < 0.5$. In contrast, both the NS-level theories overpredict the simulation data even at $e = 0.9$, and the quantitative disagreement worsens significantly with further decrease of restitution coefficient. It is surprising that the NS theory of Jenkins & Richman provides a better quantitative prediction for p and μ in comparison to Garzo and Lutsko's theory, since the latter theory incorporates the fourth velocity cumulant α_2 and makes no assumption about the smallness of the restitution coefficient.

On the whole, figures 10 and 11 confirm that the present anisotropic Gaussian theory provides better prediction for all transport coefficients ($\mathscr{N}_1$, μ and p) for the whole range of restitution coefficients in comparison to two existing theories (in the dilute limit) that are based on (i) the Chapman–Enskog expansion (Sela *et al.* 1996) and (ii) the isotropic version of Grad's moment expansion (Kremer & Marques 2011; Garzo 2012).

6. Constitutive relation for granular heat flux in the dilute limit

Lastly, we outline a procedure to derive the constitutive relation for granular heat flux focusing on the dilute limit of granular shear flow. Note that the heat flux vanishes in the uniform shear state since $\boldsymbol{\nabla} T = 0$, and hence we need to consider non-uniform shear flow ('non-USF') in which the gradients of hydrodynamic fields are non-zero, i.e. $\boldsymbol{\nabla}(n, T, \dot{\gamma}) \neq 0$. Carrying out an orthonormal expansion around the anisotropic Gaussian state, we will show that the heat-flux vector depends on the gradients of temperature and the second-moment tensor, and the thermal conductivity is characterized by an anisotropic second-rank tensor.

6.1. *Distribution function for non-uniform shear flow: expansion around the anisotropic Gaussian*

Following Grad (1949), we choose $(1, C_x, C_y, C_x^2, C_xC_y, C_y^2, C^2C_x, C^2C_y)$ as the basis set that incorporates the third-degree polynomials. Let us define an inner product,

$$\langle \chi, \psi \rangle = \frac{1}{2\pi|\boldsymbol{M}|^{1/2}} \int \chi\psi \exp\left(-\frac{1}{2}\boldsymbol{C}\cdot\boldsymbol{M}^{-1}\cdot\boldsymbol{C}\right) \mathrm{d}\boldsymbol{C}, \tag{6.1}$$

with respect to the anisotropic Gaussian as the weight function. The related orthonormal basis $(1, \xi_x, \xi_y, \xi_x^2, \xi_x\xi_y, \xi_y^2, \xi^2\xi_x, \xi^2\xi_y)$ is obtained by applying the Gram–Schmidt orthogonalization procedure.

We assume that the single-particle distribution function for the non-uniform shear flow (non-USF) can be expanded as

$$f = f_0(a + a_i\xi_i + a_{ij}\xi_i\xi_j + b_i\xi^2\xi_i), \tag{6.2}$$

where the anisotropic Gaussian

$$f_0 = \frac{n}{2\pi|\boldsymbol{M}|^{1/2}} \exp\left(-\frac{1}{2}C_\alpha M_{\alpha\beta}^{-1}C_\beta\right) \tag{6.3}$$

is the zeroth state representing the USF. The coefficients a, a_i, a_{ij} and b_i in (6.2) are to be chosen such that the basic hydrodynamic fields

$$(n, \boldsymbol{u}, \langle \boldsymbol{CC}\rangle) \tag{6.4}$$

are recovered at any order. This implies that the following 'compatibility' conditions must be satisfied:

$$\left.\begin{aligned} n(\boldsymbol{x}, t) &= \int f(\boldsymbol{c}, \boldsymbol{x}, t)\,\mathrm{d}\boldsymbol{c} = \int f_0(\boldsymbol{c}, \boldsymbol{x}, t)\,\mathrm{d}\boldsymbol{c}, \\ \int \boldsymbol{C} f(\boldsymbol{c}, \boldsymbol{x}, t)\,\mathrm{d}\boldsymbol{c} &= 0 = \int \boldsymbol{C} f_0(\boldsymbol{c}, \boldsymbol{x}, t)\,\mathrm{d}\boldsymbol{c}, \\ M_{\alpha\beta} = \int C_\alpha C_\beta f(\boldsymbol{c}, \boldsymbol{x}, t)\,\mathrm{d}\boldsymbol{c} &= \int C_\alpha C_\beta f_0(\boldsymbol{c}, \boldsymbol{x}, t)\,\mathrm{d}\boldsymbol{c} = M_{\alpha\beta}^{(0)}. \end{aligned}\right\} \tag{6.5}$$

This yields $a = 1$, $a_i = 0$, $a_{ij} = 0$ and $b_i \neq 0$. Therefore, the distribution function for non-USF is given by

$$\begin{aligned} f = \frac{n}{2\pi|\boldsymbol{M}|^{1/2}} \exp\left(-\frac{1}{2}C_\alpha M_{\alpha\beta}^{-1}C_\beta\right) \Bigg[1 &+ \frac{q_x\{C_x^3 + C_xC_y^2 - (3M_{xx} + M_{yy})C_x - 2M_{xy}C_y\}}{\rho\{M_{xx}(3M_{xx}^2 + 6M_{xy}^2 + M_{yy}^2) + 2M_{xy}^2M_{yy}\}} \\ &+ \frac{q_y\{M_{xx}(3M_{xx}^2 + 6M_{xy}^2 + M_{yy}^2) + 2M_{xy}^2M_{yy}\} - q_xM_{xy}(3M_{xx}^2 + 2M_{xx}M_{yy} + 4M_{xy}^2 + 3M_{yy}^2)}{\rho(M_{xx}M_{yy} - M_{xy}^2)\{M_{xx}^2(3M_{xx}^2 + 12M_{xy}^2 + 10M_{yy}^2) - 4M_{xy}^2(2M_{xx}M_{yy} - 4M_{xy}^2 - 3M_{yy}^2) + 3M_{yy}^4\}} \\ &\times \Bigg\{ C_x^2C_y + C_y^3 + \frac{3M_{xy}(M_{xx} + M_{yy})^3}{M_{xx}(3M_{xx}^2 + 6M_{xy}^2 + M_{yy}^2) + 2M_{xy}^2M_{yy}} C_x \\ &- \frac{M_{xx}^2(3M_{xx}^2 + 9M_{yy}M_{xx} + M_{yy}^2) + M_{xx}M_{yy}(3M_{yy}^2 + 16M_{xy}^2) - 8M_{xy}^4}{M_{xx}(3M_{xx}^2 + 6M_{xy}^2 + M_{yy}^2) + 2M_{xy}^2M_{yy}} C_y \\ &- \frac{M_{xy}(4M_{xy}^2 + 3M_{xx}^2 + 3M_{yy}^2 + 2M_{xx}M_{yy})}{M_{xx}(3M_{xx}^2 + 6M_{xy}^2 + M_{yy}^2) + 2M_{xy}^2M_{yy}} (C_x^3 + C_xC_y^2) \Bigg\} \Bigg], \end{aligned} \tag{6.6}$$

where

$$q_\alpha = \frac{m}{2}\int C^2 C_\alpha f(\boldsymbol{c},\boldsymbol{x},t)\,\mathrm{d}\boldsymbol{c} \tag{6.7}$$

is the 'kinetic' heat-flux vector.

6.2. *Generalized Fourier law from the balance of contracted third moment*

In the dilute limit, the collisional fluxes ($\varTheta(\cdot)=0$) are neglected and hence the balance equation for the contracted third moment $M_{\alpha\beta\beta}=\langle C_\alpha C_\beta C_\beta\rangle$ is obtained from (2.10) as

$$\rho\frac{\mathrm{D}M_{\alpha\beta\beta}}{\mathrm{D}t} + Q_{n\alpha\beta\beta,n} - 3M_{(\alpha\beta}P_{\beta)n,n} + 3Q_{n(\alpha\beta}u_{\beta),n} = \aleph_{\alpha\beta\beta}, \tag{6.8}$$

where $Q_{n\alpha\beta}\equiv\rho M_{n\alpha\beta}$ and the second term on the left-hand side is a contracted fourth-order moment,

$$Q_{n\alpha\beta\beta} = m\int C_n C_\alpha C^2 f(\boldsymbol{x},\boldsymbol{c},t)\,\mathrm{d}\boldsymbol{c}, \tag{6.9}$$

and the subscript under $(\ldots)$ on the third and fourth terms is defined such that

$$Q_{n(\alpha\beta}u_{\beta),n} = \tfrac{1}{3}(2Q_{n\alpha\beta}u_{\beta,n} + Q_{n\beta\beta}u_{\alpha,n}), \tag{6.10}$$

$$M_{(\alpha\beta}P_{\beta)n,n} = \tfrac{1}{3}(2M_{\alpha\beta}P_{\beta n,n} + M_{\beta\beta}P_{\alpha n,n}), \tag{6.11}$$

with the comma on the subscript denoting a partial derivative. The source term in (6.8) has the following integral expression:

$$\aleph_{\alpha\beta\beta}\equiv\aleph[C_\alpha C_\beta C_\beta] = \frac{m\sigma}{2}\iiint_{\boldsymbol{g}\cdot\boldsymbol{k}>0}\Delta(C^2C_\alpha)f(\boldsymbol{c}_1,\boldsymbol{x})f(\boldsymbol{c}_2,\boldsymbol{x})(\boldsymbol{g}\cdot\boldsymbol{k})\,\mathrm{d}\boldsymbol{k}\,\mathrm{d}\boldsymbol{c}_1\,\mathrm{d}\boldsymbol{c}_2, \tag{6.12}$$

where $\Delta(C^2C_\alpha)$ is defined in § A.3.

Inserting the distribution function (6.6) into (6.12), changing to new integration variables $(\boldsymbol{c}_1,\boldsymbol{c}_2)\to(\boldsymbol{g},\boldsymbol{G})$, and evaluating the integrals over $\boldsymbol{G}$, $\boldsymbol{g}$ and $\boldsymbol{k}$ (see § A.3), we obtain

$$\aleph_{\alpha\beta\beta} = -\frac{\rho(1+e)\sqrt{T}}{32\rho_p\sigma\sqrt{\pi}}\varOmega_{\alpha\gamma}q_\gamma, \tag{6.13}$$

where $\boldsymbol{q}=(q_x,q_y)$ is the heat-flux vector. Note that we have neglected quadratic nonlinear terms in q_γ to derive (6.13). The elements of $\varOmega=[\varOmega_{\alpha\gamma}]$ are

$$\varOmega=[\varOmega_{\alpha\gamma}] = \frac{1}{1+\eta^2+\eta^4}\begin{bmatrix}\overline{\varOmega}_{11} & \overline{\varOmega}_{12}\\ \overline{\varOmega}_{21} & \overline{\varOmega}_{22}\end{bmatrix}, \tag{6.14}$$

where

$$\left.\begin{aligned}
\overline{\varOmega}_{11} &= 608+714\eta^2+831\eta^4+82\eta^6-e(480+594\eta^2+606\eta^4-33\eta^6)\\
&\quad+\eta\sin2\phi(160+124\eta^2+148\eta^4+105\eta^6+e(-96+63\eta^2-84\eta^4)),\\
\overline{\varOmega}_{12} &= -\eta\cos2\phi(160+124\eta^2+148\eta^4+105\eta^6+e(-96+63\eta^2-84\eta^4))\\
&= \overline{\varOmega}_{21}\\
\overline{\varOmega}_{22} &= 608+714\eta^2+831\eta^4+82\eta^6-e(480+594\eta^2+606\eta^4-33\eta^6)\\
&\quad-\eta\sin2\phi(160+124\eta^2+148\eta^4+105\eta^6+e(-96+63\eta^2-84\eta^4)).
\end{aligned}\right\} \tag{6.15}$$

It is clear from (6.13) that the source term $\aleph_{\alpha\beta\beta}$ is a combination of q_x and q_y and depends on the restitution coefficient e, the temperature anisotropy η and the non-coaxiality angle ϕ.

6.2.1. *Heat flux from Maxwell iteration: thermal conductivity tensor*

Now we apply the well-known Maxwell iteration scheme (Truesdell & Muncaster 1980) to the contracted third-moment equation (6.8) to obtain the constitutive relation for heat flux. For this purpose, we rewrite (6.8) as

$$\aleph_{\alpha\beta\beta}=2\frac{\mathrm{D}q_\alpha}{\mathrm{D}t}+2q_\alpha\frac{\partial u_\beta}{\partial x_\beta}+\frac{\partial Q_{n\alpha\beta\beta}}{\partial x_n}-2(M_{\alpha\beta}+T\delta_{\alpha\beta})\frac{\partial P_{\beta n}}{\partial x_n}+2(Q_{n\alpha\beta}+q_n\delta_{\alpha\beta})\frac{\partial u_\beta}{\partial x_n}, \quad (6.16)$$

where q_α is defined in (6.7). In the Maxwell iteration scheme, the terms on the right-hand side of (6.16) are replaced by their zeroth-order values obtained by using the anisotropic Gaussian (6.3) as the distribution function. For the USF (i.e. at the zeroth order), it is straightforward to verify that

$$\left.\begin{aligned} P_{\alpha\beta}^{(0)} &= \rho M_{\alpha\beta}^{(0)}\equiv\rho M_{\alpha\beta},\\ q_\alpha^{(0)} &= 0=Q_{\alpha\beta\gamma}^{(0)},\\ Q_{n\alpha\beta\beta}^{(0)} &= 2\rho(T\delta_{\alpha\beta}+M_{\alpha\beta})M_{n\beta}, \end{aligned}\right\} \quad (6.17)$$

and hence

$$\left.\begin{aligned} M_{\alpha\beta}^{(0)}P_{\beta n,n}^{(0)} &= \frac{\partial\rho}{\partial x_n}M_{\alpha\beta}M_{\beta n}+\rho M_{\alpha\beta}\frac{\partial M_{\beta n}}{\partial x_n},\\ \frac{1}{2}Q_{n\alpha\beta\beta,n}^{(0)} &= \frac{\partial\rho}{\partial x_n}TM_{n\alpha}+\rho\frac{\partial T}{\partial x_n}M_{n\alpha}+\rho T\frac{\partial M_{n\alpha}}{\partial x_n}\\ &\quad+\frac{\partial\rho}{\partial x_n}M_{n\beta}M_{\alpha\beta}+\rho\frac{\partial M_{n\beta}}{\partial x_n}M_{\alpha\beta}+\rho M_{n\beta}\frac{\partial M_{\alpha\beta}}{\partial x_n}. \end{aligned}\right\} \quad (6.18)$$

Inserting (6.17) and (6.18) into the right-hand side of (6.16) and equating the resulting expression with (6.13), we obtain the desired constitutive relation for the heat flux:

$$q_\gamma=-\frac{64\rho_p\sigma\sqrt{\pi}}{(1+e)\sqrt{T}}\,\mathfrak{Q}_{\gamma\alpha}^{-1}\left(2M_{\alpha n}\frac{\partial T}{\partial x_n}+M_{\beta n}\frac{\partial\widehat{M}_{\alpha\beta}}{\partial x_n}\right), \quad (6.19)$$

where $\widehat{M}_{\alpha\beta}$ is the deviatoric part of the second-moment tensor $M_{\alpha\beta}=T\delta_{\alpha\beta}+\widehat{M}_{\alpha\beta}$, with $\mathfrak{Q}_{\gamma\alpha}$ being given by (6.14) and (6.15). (A similar expression for the heat flux was used by Simon & Jenkins (1994) in the context of modelling planetary rings, made of inelastic spheres (i.e. in three dimensions), but they did not present the related derivation.) Equation (6.19) should be treated as a generalized Fourier law, since the gradient of the deviatoric part of the second moment (or the kinetic stress) also creates a heat flux, in addition to the standard Fourier contribution due to the temperature gradient. This indicates that there could be a heat flux even in the absence of a temperature gradient, driven solely by the gradient of the deviatoric stress $\widehat{M}_{\alpha\beta}$. Such a stress-gradient-driven heat flux is well known in rarefied gases (Grad 1949; Kogan 1969; Chapman & Cowling 1970); in fact, applying the Maxwell iteration scheme to equation (5.38) of Grad (1949) leads to a similar constitutive relation for the heat flux as in (6.19). In any case, identifying the coefficient of the temperature gradient in (6.19) with the thermal conductivity, we find that the thermal conductivity,

$$\kappa_{\gamma n}=\frac{128\rho_p\sigma\sqrt{\pi}}{(1+e)\sqrt{T}}\,\mathfrak{Q}_{\gamma\alpha}^{-1}M_{\alpha n}, \quad (6.20)$$

is a second-rank tensor that is anisotropic ($\kappa_{xx} \neq \kappa_{yy}$ and $\kappa_{xy} \neq 0$). The anisotropy of (6.20) is a consequence of the imposed shear field, since the 'cross' thermal conductivity coefficient κ_{xy} is proportional to $\eta \sim \dot{\gamma}$. Therefore, (6.20) can aptly be dubbed the 'shear-induced' anisotropic thermal conductivity tensor. One consequence of this anisotropy is the well-known rarefaction effect of heat flow along a direction orthogonal to the temperature gradient (Kogan 1969).

6.2.2. *Thermal conductivity at Navier–Stokes order: verification*

As a check, we consider the limit of vanishing temperature anisotropy, $\eta \to 0$, for which the following relations hold:

$$M_{\alpha\beta} = T\delta_{\alpha\beta}, \quad \widehat{M}_{\alpha\beta} = 0 \quad \text{and} \quad \mathfrak{Q}^{-1}_{\gamma\alpha} = \frac{-1}{32(15e-19)}\delta_{\gamma\alpha}. \tag{6.21a–c}$$

Inserting these into (6.19) and (6.20), we obtain

$$q_\gamma = -\frac{16m\sqrt{T}}{\sqrt{\pi}\sigma(19+4e-15e^2)}\frac{\partial T}{\partial x_\gamma} \equiv -\kappa\frac{\partial T}{\partial x_\gamma}, \tag{6.22}$$

where

$$\kappa = \frac{16m\sqrt{T}}{\sqrt{\pi}\sigma(19+4e-15e^2)}. \tag{6.23}$$

Equation (6.23) agrees exactly with the expression for thermal conductivity for a dilute system of inelastic hard disks at NS order (Jenkins & Richman 1985*a*).

To summarize this section, we have found a generalized Fourier law (6.19) and determined the explicit expressions for the elements of the thermal conductivity tensor (6.20) in terms of e, η and ϕ for a sheared system of a dilute granular gas in two dimensions. This should be extended to a dense granular gas to obtain an expression for the thermal conductivity tensor for the whole range of densities.

7. Conclusions and outlook

We analysed the Grad-level moment equations (Grad 1949; Jenkins & Richman 1988) for the plane shear flow of smooth inelastic disks, with a goal to obtain closed-form expressions for the non-Newtonian stress tensor, the collisional dissipation rate and the granular heat flux. In this moment approach, an anisotropic Gaussian (Goldreich & Tremaine 1978; Araki & Tremaine 1986), which is a function of all components of the second moment of the fluctuation velocity ($\boldsymbol{M} = \langle \boldsymbol{CC} \rangle$), was taken as the single-particle distribution function representing the base state of USF. The mass and momentum balance equations are identically satisfied for USF, and the equation for the second-moment tensor of velocity fluctuations was solved semi-analytically via a series expansion of certain collision integrals.

We derived closed-form expressions for all the transport coefficients (shear viscosity μ, pressure p and first normal stress difference $\mathscr{N}_1$) and the collisional dissipation rate $\mathscr{D}$ in terms of five parameters: (i) density or area fraction ν, (ii) restitution coefficient e, (iii) shear rate R (see (3.10)), (iv) temperature anisotropy η (see (3.6)) and (v) angle ϕ between the principal eigenvectors of the shear tensor $\boldsymbol{D} = (\boldsymbol{\nabla u} + (\boldsymbol{\nabla u})^{\mathrm{T}})/2$ and the second-moment tensor $\boldsymbol{M}$. The last two parameters (η and ϕ) are zero at the NS order (i.e. at the linear order in the shear rate) and are, therefore, a measure of the non-Newtonian rheology of the medium. In the uniform shear state, we found that R, η

and $\sin 2\phi$ scale with inelasticity $\epsilon = (1-e)^{1/2}$ at the leading order (see (4.6) and discussion in § 4.4), and therefore the shear-rate dependence of transport coefficients can be translated into their dependence on ϵ in USF. The nonlinear nature of the rheology was analysed by retaining terms up to the super-Burnett order (i.e. third order in R and η) in the transport coefficients, and our analytical expressions for transport coefficients reduced to known exact expressions for the Newtonian rheology when they were truncated at the NS order. The origin of the first normal stress difference was shown to be tied to (i) the non-coaxiality ($\phi \neq 0$) of the principal directions of the shear and second-moment tensors and (ii) the temperature anisotropy ($\eta \neq 0$). Both are shear-induced effects and appear at the Burnett-order approximation of transport coefficients. In particular, both $\sin 2\phi$ and η are finite and are of the same order in the dilute limit, leading to $\mathscr{N}_1 \neq 0$ as $\nu \to 0$.

From a comparison of analytically derived constitutive relations with those obtained from the full numerical solution of moment equations (see figure 3), we showed that, while the Burnett-order terms (i.e. second order in R and η) are sufficient for accurate predictions of all transport coefficients (μ, p and $\mathscr{N}_1$) in the dilute limit, the super-Burnett-order terms must be retained to achieve similar accuracy for dense flows, especially at large dissipations. The resulting super-Burnett-order transport coefficients were further validated via a comparison with the event-driven simulation data for the USF of an inelastic hard-disk system. We found good agreement between simulation and moment theory for p, μ and $\mathscr{N}_1$ (figures 5–9) for a range of densities spanning from the dilute to close to the freezing point. In contrast, the transport coefficients obtained from an NS-order constitutive model (which is assumed to hold at any dissipation (Lutsko 2005; Garzo *et al.* 2007)) were shown to deviate significantly from both simulation and the moment theory even at moderate values of the restitution coefficient ($e \sim 0.9$). The success of the anisotropic Gaussian to predict transport coefficients in the uniform shear state seems to be tied to the fact that the terms of all orders in the shear rate and the temperature anisotropy are implicitly incorporated in the anisotropic Gaussian distribution function.

Going beyond the uniform shear state, we derived a constitutive relation for the granular heat flux in the dilute limit (§ 6) using a perturbation expansion around the anisotropic Gaussian and subsequently employing the Maxwell iteration scheme on the balance equation for the contracted third moment ($M_{\alpha\beta\beta} = \langle C_\alpha C^2 \rangle$) of fluctuation velocity. We found that the granular heat flux follows a generalized Fourier law (6.19) in which the gradients of the deviatoric part of the second-moment tensor drive a heat current in addition to the standard Fourier conduction driven by the temperature gradient. This non-Fourier contribution is a rarefaction effect, which appears at the Grad-level (second order in gradients) description of the granular shear flow, and has an analogue in rarefied molecular gases too (Grad 1949). The thermal conductivity is found to be characterized by an anisotropic second-rank tensor (6.20), for which we derived an explicit expression in terms of the restitution coefficient e, temperature anisotropy η and non-coaxiality angle ϕ. In the limits of $\eta \to 0$ and $\phi \to 0$, we recovered the expression for the scalar thermal conductivity that holds at the NS order.

In addition to considering the three-dimensional case of spheres, the present anisotropic moment theory can be extended to include the full contracted fourth moment ($M_{\alpha\alpha\beta\beta} = \langle C^4 \rangle$) as a separate hydrodynamic field, which is likely to recover the density-gradient-dependent term in the constitutive relation for heat flux (Saha & Alam 2014). This will also generate additional contributions (in terms of the fourth velocity cumulant, $\alpha_2 = \langle C^4 \rangle / \langle C^4 \rangle^{(0)} - 1$) to (i) the shear viscosity μ (4.11) and (ii) the dissipation rate $\mathscr{D}$ (4.24) that can be checked in future work. For the

three-dimensional case, the existing Grad-level theories that are based on an expansion around the isotropic Gaussian state (e.g. Kremer & Marques 2011) predict that the second normal stress difference is zero, which is in contrast to both the particle simulation data (Alam & Luding 2005*a*,*b*) and the Burnett-order theory (Sela & Goldhirsch 1998) based on Chapman–Enskog expansion. On the other hand, the theories based on the anisotropic Gaussian (Chou & Richman 1998; Lutsko 2004) predict non-zero values for both normal stress differences. Therefore, the present semi-analytical formalism of the anisotropic moment theory should be extended to derive closed-form constitutive relations for spheres too. Another direction of research would be to extend the present approach: (i) to include the rotational motion for a rough frictional granular gas (Jenkins & Richman 1985*a*; Mitarai, Nakanishi & Hayakawa 2002; Rongali & Alam 2014); and (ii) to consider a sheared binary or polydisperse granular mixture (Alam *et al.* 2002; Lutsko 2004; Montanero *et al.* 2006). The present constitutive relations for the stress tensor (§ 4.2) and the heat flux (§ 6) along with extended hydrodynamic equations (2.11)–(2.13) can also be tested in dynamic simulations of granular flows, including the stability analyses of shear flows (Gayen & Alam 2006; Shukla & Alam 2009, 2011*a*,*b*).

Acknowledgements

One of us (M.A.) learned much about the related literature on 'planetary rings' while attending a conference on 'Non-Equilibrium Dynamics in Astrophysics and Material Science' (November 2011), held at Yukawa Institute for Theoretical Physics, Kyoto University, Japan, and is grateful to Professor H. Hayakawa for the invitation and hospitality for the same. M.A. would like to thank Professor J. T. Jenkins for a fruitful coffee-table discussion on this topic during this conference as well as Dr J. Schmidt for discussions on Saturn's ring and sharing many related references.

Appendix A. Integral expressions for collisional flux and source terms

A.1. *Collisional flux of momentum ($\Theta_{\alpha\beta}$) at second order*

For a dense system of disks, the collisional flux of momentum can be expressed as (Jenkins & Richman 1985*a*,*b*, 1988):

$$\begin{aligned}\Theta_{\alpha\beta} &= \Theta_\alpha[mC_\beta]\\ &= \frac{m(1+e)\sigma^2}{4}\iiint_{\boldsymbol{g}\cdot\boldsymbol{k}>0}(\boldsymbol{g}\cdot\boldsymbol{k})^2 k_\alpha k_\beta\\ &\quad\times\int_0^1 f^{(2)}(\boldsymbol{c}_1,\boldsymbol{x}-\omega\sigma\boldsymbol{k},\boldsymbol{c}_2,\boldsymbol{x}+\sigma\boldsymbol{k}-\omega\sigma\boldsymbol{k})\,\mathrm{d}\omega\,\mathrm{d}\boldsymbol{k}\,\mathrm{d}\boldsymbol{c}_1\,\mathrm{d}\boldsymbol{c}_2\\ &= \frac{m(1+e)\sigma^2}{4}\iiint_{\boldsymbol{g}\cdot\boldsymbol{k}>0}(\boldsymbol{g}\cdot\boldsymbol{k})^2 k_\alpha k_\beta\\ &\quad\times\int_{-1/2}^{1/2} f^{(2)}\left(\boldsymbol{c}_1,\boldsymbol{x}+\left(\xi-\frac{1}{2}\right)\sigma\boldsymbol{k},\boldsymbol{c}_2,\boldsymbol{x}+\left(\xi+\frac{1}{2}\right)\sigma\boldsymbol{k}\right)\mathrm{d}\xi\,\mathrm{d}\boldsymbol{G}\,\mathrm{d}\boldsymbol{k}\,\mathrm{d}\boldsymbol{g}.\end{aligned}\tag{A 1}$$

The latter expression has been obtained via a change of variables: $(\boldsymbol{c}_1,\,\boldsymbol{c}_2,\,\omega)\to(\boldsymbol{g},\,\boldsymbol{G},\,\xi)$, with $\boldsymbol{g}=\boldsymbol{c}_1-\boldsymbol{c}_2$, $\boldsymbol{G}=(\boldsymbol{C}_1+\boldsymbol{C}_2)/2$, $\xi=1/2-\omega$ and $\mathrm{d}\boldsymbol{c}_1\,\mathrm{d}\boldsymbol{c}_2=\mathrm{d}\boldsymbol{g}\,\mathrm{d}\boldsymbol{G}$. With the molecular chaos assumption and using the Taylor series expansion on the single-particle distribution $f^{(1)}$, the two-particle distribution in (A 1) can be

simplified to

$$f^{(2)}\left(\boldsymbol{c}_1, \boldsymbol{x}+\left(\xi-\frac{1}{2}\right)\sigma\boldsymbol{k}, \boldsymbol{c}_2, \boldsymbol{x}+\left(\xi+\frac{1}{2}\right)\sigma\boldsymbol{k}\right)$$
$$=\frac{n^2 g_0}{4\pi^2|\boldsymbol{M}|}\exp\left\{-\frac{1}{4}M^{-1}_{\alpha\beta}[(g_\alpha+V_\alpha)(g_\beta+V_\beta)+4(G_\alpha-\xi V_\alpha)(G_\beta-\xi V_\beta)]\right\}, \quad \text{(A 2)}$$

where $|\boldsymbol{M}|\equiv\det(\boldsymbol{M})$ and $\boldsymbol{V}=\sigma\boldsymbol{k}\cdot\boldsymbol{\nabla}u$.

Combining (A 1) and (A 2), we obtain

$$\begin{aligned}\Theta_{\alpha\beta} &= \frac{m(1+e)n^2 g_0\sigma^2}{16\pi^2|\boldsymbol{M}|}\iint_{\boldsymbol{g}\cdot\boldsymbol{k}>0}(\boldsymbol{g}\cdot\boldsymbol{k})^2 k_\alpha k_\beta \exp\left\{-\frac{1}{4}\left[(g_\alpha+V_\alpha)M^{-1}_{\alpha\beta}(g_\beta+V_\beta)\right]\right\}\\ &\quad\times\left(\int_{-1/2}^{1/2}\int\exp\{-[(G_\alpha-\xi V_\alpha)M^{-1}_{\alpha\beta}(G_\beta-\xi V_\beta)]\}\,\mathrm{d}\boldsymbol{G}\,\mathrm{d}\xi\right)\mathrm{d}\boldsymbol{k}\,\mathrm{d}\boldsymbol{g}\\ &= \frac{\rho n(1+e)g_0\sigma^2}{16\pi|\boldsymbol{M}|^{1/2}}\iint_{\boldsymbol{g}\cdot\boldsymbol{k}>0}(\boldsymbol{g}\cdot\boldsymbol{k})^2 k_\alpha k_\beta\exp\left\{-\frac{1}{4}[(g_\alpha+V_\alpha)M^{-1}_{\alpha\beta}(g_\beta+V_\beta)]\right\}\mathrm{d}\boldsymbol{k}\,\mathrm{d}\boldsymbol{g}.\end{aligned} \quad \text{(A 3)}$$

To arrive at (A 3), the identity $\int\int(\cdot)\,\mathrm{d}\boldsymbol{G}\,\mathrm{d}\xi=\pi\sqrt{|\boldsymbol{M}|}$ has been used. Carrying out the integration over $\boldsymbol{g}$, a compact expression for the collisional flux of momentum is obtained as given by (3.13).

A.2. *Collisional source of second moment ($\aleph_{\alpha\beta}$) at second order*

Using the molecular chaos assumption and the Taylor series expansion of a single-particle distribution about $\boldsymbol{x}$, the two-particle distribution function can be written as

$$\begin{aligned}&f^{(2)}(\boldsymbol{c}_1, \boldsymbol{x}-\sigma\boldsymbol{k}, \boldsymbol{c}_2, \boldsymbol{x})\\ &\quad=\frac{n^2 g_0}{4\pi^2|\boldsymbol{M}|}\exp\left\{-\frac{1}{2}M^{-1}_{\alpha\beta}[(C_\alpha+V_\alpha)(C_\beta+V_\beta)+(C_\alpha C_\beta)]\right\}\\ &\quad=\frac{n^2 g_0}{4\pi^2|\boldsymbol{M}|}\exp\left\{-\frac{1}{4}M^{-1}_{\alpha\beta}[(g_\alpha+V_\alpha)(g_\beta+V_\beta)+(2G_\alpha+V_\alpha)(2G_\beta+V_\beta)]\right\},\end{aligned} \quad \text{(A 4)}$$

where the last expression involves a change of variables $(\boldsymbol{c}_1, \boldsymbol{c}_2)\to(\boldsymbol{g}, \boldsymbol{G})$ and $\boldsymbol{V}=\sigma\boldsymbol{k}\cdot\boldsymbol{\nabla}\boldsymbol{u}$.

The collisional source of the second moment can be expressed as (Jenkins & Richman 1985*a*,*b*, 1988)

$$\begin{aligned}\aleph_{\alpha\beta} &\equiv \aleph_{\alpha\beta}[mC_\alpha C_\beta]\\ &= \frac{m\sigma}{2}\iiint_{\boldsymbol{g}\cdot\boldsymbol{k}>0}\Delta(C_\alpha C_\beta)f^{(2)}(\boldsymbol{c}_1, \boldsymbol{x}-\sigma\boldsymbol{k}, \boldsymbol{c}_2, \boldsymbol{x})(\boldsymbol{k}\cdot\boldsymbol{g})\,\mathrm{d}\boldsymbol{k}\,\mathrm{d}\boldsymbol{c}_1\,\mathrm{d}\boldsymbol{c}_2\\ &= \frac{mn^2 g_0\sigma}{8\pi^2|\boldsymbol{M}|}\iint_{\boldsymbol{g}\cdot\boldsymbol{k}>0}\Delta(C_\alpha C_\beta)(\boldsymbol{g}\cdot\boldsymbol{k})\exp\left\{-\frac{1}{4}[(g_\alpha+V_\alpha)M^{-1}_{\alpha\beta}(g_\beta+V_\beta)]\right\}\\ &\quad\times\left(\int\exp\left\{-\frac{1}{4}[(2G_\alpha+V_\alpha)M^{-1}_{\alpha\beta}(2G_\beta+V_\beta)]\right\}\mathrm{d}\boldsymbol{G}\right)\mathrm{d}\boldsymbol{k}\,\mathrm{d}\boldsymbol{g}\end{aligned}$$

$$= \frac{m\sigma n^2 g_0}{8\pi|\boldsymbol{M}|^{1/2}} \iint_{\boldsymbol{g}\cdot\boldsymbol{k}>0} \Delta(C_\alpha C_\beta)(\boldsymbol{g}\cdot\boldsymbol{k}) \exp\left\{-\frac{1}{4}[(g_\alpha + V_\alpha)M^{-1}_{\alpha\beta}(g_\beta + V_\beta)]\right\} \mathrm{d}\boldsymbol{k}\,\mathrm{d}\boldsymbol{g}$$

$$= \frac{\rho\nu g_0}{2\pi^2\sigma|\boldsymbol{M}|^{1/2}} \iint_{\boldsymbol{g}\cdot\boldsymbol{k}>0} \Delta(C_\alpha C_\beta)(\boldsymbol{g}\cdot\boldsymbol{k}) \exp\left\{-\frac{1}{4}[(g_\alpha + V_\alpha)M^{-1}_{\alpha\beta}(g_\beta + V_\beta)]\right\} \mathrm{d}\boldsymbol{k}\,\mathrm{d}\boldsymbol{g}. \tag{A 5}$$

The last expression results from $\int(\cdot)\,\mathrm{d}\boldsymbol{G} = \pi\sqrt{|\boldsymbol{M}|}$. Note further that

$$\Delta(C_\alpha C_\beta) = -\tfrac{1}{2}(1-e^2)(\boldsymbol{g}\cdot\boldsymbol{k})^2 k_\alpha k_\beta - \tfrac{1}{2}(1+e)(\boldsymbol{g}\cdot\boldsymbol{k})(\boldsymbol{g}\cdot\boldsymbol{j})(j_\alpha k_\beta + k_\alpha j_\beta), \tag{A 6}$$

where $\boldsymbol{j}$ is a unit vector perpendicular to the contact vector $\boldsymbol{k}$.

Inserting (A 6) into (A 5) and performing integrations over $\boldsymbol{g}$, a compact expression for $\aleph_{\alpha\beta}$ is obtained,

$$\aleph_{\alpha\beta} = A_{\alpha\beta} + \widehat{B}_{\alpha\beta}, \tag{A 7}$$

where $A_{\alpha\beta}$ is given by (3.15), and the traceless part, $\widehat{B}_{\alpha\beta}$, can be further decomposed into

$$\widehat{B}_{\alpha\beta} = \widehat{E}_{\alpha\beta} + \widehat{F}_{\alpha\beta}, \tag{A 8}$$

where

$$\widehat{E}_{\alpha\beta} = -\frac{4(1+e)\rho\nu g_0(\nu)}{\sigma\pi^{3/2}} \int (j_\alpha k_\beta + k_\alpha j_\beta)(\boldsymbol{j}\cdot\boldsymbol{M}\cdot\boldsymbol{k})(\boldsymbol{k}\cdot\boldsymbol{M}\cdot\boldsymbol{k})^{1/2}\mathfrak{F}(\chi)\,\mathrm{d}\boldsymbol{k}, \tag{A 9}$$

$$\begin{aligned}\widehat{F}_{\alpha\beta} &= \frac{2(1+e)\rho\nu g_0(\nu)}{\sigma\pi^{3/2}} \int (j_\alpha k_\beta + k_\alpha j_\beta)(\boldsymbol{V}\cdot\boldsymbol{M}^{-1}\cdot\boldsymbol{j})|\boldsymbol{M}|\mathfrak{G}(\chi)\,\mathrm{d}\boldsymbol{k} \\ &= \frac{2(1+e)\rho\nu g_0(\nu)}{\pi^{3/2}} \int (j_\alpha k_\beta + k_\alpha j_\beta)(\boldsymbol{k}\cdot(\boldsymbol{W}+\boldsymbol{D})\cdot\boldsymbol{M}^{-1}\cdot\boldsymbol{j})|\boldsymbol{M}|\mathfrak{G}(\chi)\,\mathrm{d}\boldsymbol{k} \\ &= \Theta_{\alpha\gamma}W_{\beta\gamma} + \Theta_{\beta\gamma}W_{\alpha\gamma} + \widehat{G}_{\alpha\beta},\end{aligned} \tag{A 10}$$

and

$$\widehat{G}_{\alpha\beta} = \frac{2(1+e)\rho\nu g_0(\nu)}{\pi^{3/2}} \int (j_\alpha k_\beta + k_\alpha j_\beta)k_\xi j_\gamma (TD_{\gamma\xi} - D_{\delta\xi}\widehat{M}_{\delta\gamma})\mathfrak{G}(\chi)\,\mathrm{d}\boldsymbol{k}, \tag{A 11}$$

with $\widehat{\boldsymbol{M}}$ being the deviatoric part of $\boldsymbol{M}$. The expression for $\mathfrak{F}(\chi)$ is given by (3.18), with χ as in (3.20).

A.3. *Third-order source term ($\aleph_{\alpha\beta\beta}$) to calculate heat flux in the dilute limit*

In the dilute limit, the third-order source term in (6.8) has the following integral expression:

$$\begin{aligned}\aleph_{\alpha\beta\beta} &= \aleph[mC^2C_\alpha] \\ &= \frac{m\sigma}{2} \iiint_{\boldsymbol{g}\cdot\boldsymbol{k}>0} \Delta(C^2C_\alpha) f^{(1)}(\boldsymbol{c}_1,\boldsymbol{x}) f^{(1)}(\boldsymbol{c}_2,\boldsymbol{x})(\boldsymbol{g}\cdot\boldsymbol{k})\,\mathrm{d}\boldsymbol{k}\,\mathrm{d}\boldsymbol{c}_1\,\mathrm{d}\boldsymbol{c}_2.\end{aligned} \tag{A 12}$$

Changing the variables of integration from $(\boldsymbol{c}_1,\boldsymbol{c}_2)\to(\boldsymbol{g},\boldsymbol{G})$, with $\mathrm{d}\boldsymbol{c}_1\,\mathrm{d}\boldsymbol{c}_2 = \mathrm{d}\boldsymbol{C}_1\,\mathrm{d}\boldsymbol{C}_2 = \mathrm{d}\boldsymbol{g}\,\mathrm{d}\boldsymbol{G}$ and

$$\begin{aligned}\Delta(C^2C_\alpha) = {} & [(1+e)^2(\boldsymbol{g}\cdot\boldsymbol{k})^2 G_\beta k_\beta k_\alpha - \tfrac{1}{2}(1-e^2)(\boldsymbol{g}\cdot\boldsymbol{k})^2 G_\alpha \\ & - (1+e)(\boldsymbol{g}\cdot\boldsymbol{k})G_\beta(k_\beta g_\alpha + g_\beta k_\alpha)],\end{aligned} \tag{A 13}$$

we can write

$$\begin{aligned}\aleph_{\alpha\beta\beta} &= \frac{m\sigma n^2}{8\pi^2|\boldsymbol{M}|}\iiint_{\boldsymbol{g}\cdot\boldsymbol{k}>0}\Big[(1+e)^2(\boldsymbol{g}\cdot\boldsymbol{k})^3G_\beta k_\beta k_\alpha \\ &\quad -\frac{1}{2}(1-e^2)(\boldsymbol{g}\cdot\boldsymbol{k})^3G_\alpha-(1+e)(\boldsymbol{g}\cdot\boldsymbol{k})^2G_\beta(k_\beta g_\alpha+g_\beta k_\alpha)\Big] \\ &\quad\times\exp\left\{-\frac{1}{4}M_{ab}^{-1}(4G_aG_b+g_ag_b)\right\}[Xf_1(\boldsymbol{g},\boldsymbol{G})+Yf_2(\boldsymbol{g},\boldsymbol{G})]\,\mathrm{d}\boldsymbol{G}\,\mathrm{d}\boldsymbol{g}\,\mathrm{d}\boldsymbol{k} \\ &\equiv I^{(1)}_{\alpha\beta\beta}+I^{(2)}_{\alpha\beta\beta}+I^{(3)}_{\alpha\beta\beta},\end{aligned} \tag{A 14}$$

where

$$X=\frac{q_x}{2\rho(M_{xx}(3M_{xx}^2+6M_{xy}^2+M_{yy}^2)+2M_{xy}^2M_{yy})}, \tag{A 15}$$

$$Y=\frac{q_y(M_{xx}(3M_{xx}^2+6M_{xy}^2+M_{yy}^2)+2M_{xy}^2M_{yy})-q_xM_{xy}(3M_{xx}^2+2M_{xx}M_{yy}+4M_{xy}^2+3M_{yy}^2)}{\rho|\boldsymbol{M}|(M_{xx}^2(3M_{xx}^2+12M_{xy}^2+10M_{yy}^2)+4M_{xy}^2(-2M_{xx}M_{yy}+4M_{xy}^2+3M_{yy}^2)+3M_{yy}^4)} \tag{A 16}$$

$$f_1(\boldsymbol{g},\boldsymbol{G}) = \{3g_x^2G_x+g_y^2G_x+4G_x^3+2g_xg_yG_y+4G_xG_y^2-4(3M_{xx}+M_{yy})G_x-8M_{xy}G_y\}, \tag{A 17}$$

$$\begin{aligned}f_2(\boldsymbol{g},\boldsymbol{G}) &= \left\{\frac{3}{2}g_y^2G_y+\frac{1}{2}g_x^2G_y+2G_y^3+g_xg_yG_x+2G_x^2G_y\right. \\ &\quad+\frac{6M_{xy}(M_{xx}+M_{yy})^3}{3M_{xx}^3+6M_{xy}^2M_{xx}+M_{xx}M_{yy}^2+2M_{xy}^2M_{yy}}G_x \\ &\quad-\frac{2(3M_{xx}^4+9M_{yy}M_{xx}^3+M_{yy}^2M_{xx}^2+3M_{yy}^3M_{xx}+16M_{xy}^2M_{yy}M_{xx}-8M_{xy}^4)}{3M_{xx}^3+6M_{xy}^2M_{xx}+M_{yy}^2M_{xx}+2M_{xy}^2M_{yy}}G_y \\ &\quad-\frac{M_{xy}(4M_{xy}^2+3M_{xx}^2+3M_{yy}^2+2M_{xx}M_{yy})}{3M_{xx}^3+6M_{xy}^2M_{xx}+M_{yy}^2M_{xx}+2M_{xy}^2M_{yy}} \\ &\quad\times\left.\left(\frac{3}{2}g_x^2G_x+\frac{1}{2}g_y^2G_x+2G_x^3+g_xg_yG_y+2G_xG_y^2\right)\right\}.\end{aligned} \tag{A 18}$$

Now using

$$\int\exp\{-G_aM_{ab}^{-1}G_b\}\,\mathrm{d}\boldsymbol{G}=\pi|\boldsymbol{M}|^{1/2}, \tag{A 19}$$

$$\int G_iG_j\exp\{-G_aM_{ab}^{-1}G_b\}\,\mathrm{d}\boldsymbol{G}=\frac{\pi}{2}|\boldsymbol{M}|^{1/2}M_{ij}, \tag{A 20}$$

$$\int G_iG_jG_kG_l\exp\{-G_aM_{ab}^{-1}G_b\}\,\mathrm{d}\boldsymbol{G}=\frac{\pi}{4}|\boldsymbol{M}|^{1/2}(M_{ij}M_{kl}+M_{ik}M_{jl}+M_{il}M_{jk}), \tag{A 21}$$

we carry out the integrations over $\boldsymbol{G}$ to obtain

$$\begin{aligned}I^{(1)}_{\alpha\beta\beta} &= \frac{m\sigma n^2(1+e)^2}{8\pi|\boldsymbol{M}|^{1/2}}\iint_{\boldsymbol{g}\cdot\boldsymbol{k}>0}\exp\left\{-\frac{1}{4}g_aM_{ab}^{-1}g_b\right\}(\boldsymbol{g}\cdot\boldsymbol{k})^3k_\beta k_\alpha \\ &\quad\times\left[X\left(\frac{3}{2}g_x^2M_{x\beta}+\frac{1}{2}g_y^2M_{x\beta}+g_xg_yM_{y\beta}-(3M_{xx}+M_{yy})M_{x\beta}-2M_{xy}M_{y\beta}\right)\right.\end{aligned}$$

$$+Y\left\{\frac{3}{4}g_y^2M_{y\beta}+\frac{1}{4}g_x^2M_{y\beta}+\frac{1}{2}g_xg_yM_{x\beta}+\frac{1}{2}(M_{xx}+3M_{yy})M_{y\beta}+M_{xy}M_{x\beta}\right.$$
$$+\frac{3M_{xy}M_{x\beta}(M_{xx}+M_{yy})^3}{3M_{xx}^3+6M_{xy}^2M_{xx}+M_{xx}M_{yy}^2+2M_{xy}^2M_{yy}}$$
$$-\frac{(3M_{xx}^4+9M_{yy}M_{xx}^3+M_{yy}^2M_{xx}^2+3M_{yy}^3M_{xx}+16M_{xy}^2M_{yy}M_{xx}-8M_{xy}^4)}{3M_{xx}^3+6M_{xy}^2M_{xx}+M_{yy}^2M_{xx}+2M_{xy}^2M_{yy}}M_{y\beta}$$
$$-\frac{4M_{xy}^3+3M_{xx}^2M_{xy}+3M_{yy}^2M_{xy}+2M_{xx}M_{yy}M_{xy}}{3M_{xx}^3+6M_{xy}^2M_{xx}+M_{yy}^2M_{xx}+2M_{xy}^2M_{yy}}$$
$$\left.\left.\times\left(\frac{3}{4}g_x^2M_{x\beta}+\frac{1}{4}g_y^2M_{x\beta}+\frac{1}{2}g_xg_yM_{y\beta}+\frac{1}{2}(3M_{xx}+M_{yy})M_{x\beta}+M_{xy}M_{y\beta}\right)\right\}\right]\mathrm{d}\boldsymbol{g}\,\mathrm{d}\boldsymbol{k},\tag{A 22}$$

$$I_{\alpha\beta\beta}^{(2)}=-\frac{m\sigma n^2(1-e^2)}{16\pi|\boldsymbol{M}|^{1/2}}\iint_{\boldsymbol{g}\cdot\boldsymbol{k}>0}\exp\left\{-\frac{1}{4}g_aM_{ab}^{-1}g_b\right\}(\boldsymbol{g}\cdot\boldsymbol{k})^3$$
$$\times\left[X\left(\frac{3}{2}g_x^2M_{x\alpha}+\frac{1}{2}g_y^2M_{x\alpha}+g_xg_yM_{y\alpha}-(3M_{xx}+M_{yy})M_{x\alpha}-2M_{xy}M_{y\alpha}\right)\right.$$
$$+Y\left\{\frac{3}{4}g_y^2M_{y\alpha}+\frac{1}{4}g_x^2M_{y\alpha}+\frac{1}{2}g_xg_yM_{x\alpha}+\frac{1}{2}(M_{xx}+3M_{yy})M_{y\alpha}+M_{xy}M_{x\alpha}\right.$$
$$+\frac{3M_{xy}M_{x\alpha}(M_{xx}+M_{yy})^3}{3M_{xx}^3+6M_{xy}^2M_{xx}+M_{xx}M_{yy}^2+2M_{xy}^2M_{yy}}$$
$$-\frac{(3M_{xx}^4+9M_{yy}M_{xx}^3+M_{yy}^2M_{xx}^2+3M_{yy}^3M_{xx}+16M_{xy}^2M_{yy}M_{xx}-8M_{xy}^4)}{3M_{xx}^3+6M_{xy}^2M_{xx}+M_{yy}^2M_{xx}+2M_{xy}^2M_{yy}}M_{y\alpha}$$
$$-\frac{4M_{xy}^3+3M_{xx}^2M_{xy}+3M_{yy}^2M_{xy}+2M_{xx}M_{yy}M_{xy}}{3M_{xx}^3+6M_{xy}^2M_{xx}+M_{yy}^2M_{xx}+2M_{xy}^2M_{yy}}$$
$$\left.\left.\times\left(\frac{3}{4}g_x^2M_{x\alpha}+\frac{1}{4}g_y^2M_{x\alpha}+\frac{1}{2}g_xg_yM_{y\alpha}+\frac{1}{2}(3M_{xx}+M_{yy})M_{x\alpha}+M_{xy}M_{y\alpha}\right)\right\}\right]\mathrm{d}\boldsymbol{g}\,\mathrm{d}\boldsymbol{k},\tag{A 23}$$

$$I_{\alpha\beta\beta}^{(3)}=-\frac{m\sigma n^2(1+e)}{8\pi|\boldsymbol{M}|^{1/2}}\iint_{\boldsymbol{g}\cdot\boldsymbol{k}>0}\exp\left\{-\frac{1}{4}g_aM_{ab}^{-1}g_b\right\}(\boldsymbol{g}\cdot\boldsymbol{k})^2(k_\beta g_\alpha+g_\beta k_\alpha)$$
$$\times\left[X\left(\frac{3}{2}g_x^2M_{x\beta}+\frac{1}{2}g_y^2M_{x\beta}+g_xg_yM_{y\beta}-(3M_{xx}+M_{yy})M_{x\beta}-2M_{xy}M_{y\beta}\right)\right.$$
$$+Y\left\{\frac{3}{4}g_y^2M_{y\beta}+\frac{1}{4}g_x^2M_{y\beta}+\frac{1}{2}g_xg_yM_{x\beta}+\frac{1}{2}(M_{xx}+3M_{yy})M_{y\beta}+M_{xy}M_{x\beta}\right.$$
$$+\frac{3M_{xy}M_{x\beta}(M_{xx}+M_{yy})^3}{3M_{xx}^3+6M_{xy}^2M_{xx}+M_{xx}M_{yy}^2+2M_{xy}^2M_{yy}}$$
$$-\frac{(3M_{xx}^4+9M_{yy}M_{xx}^3+M_{yy}^2M_{xx}^2+3M_{yy}^3M_{xx}+16M_{xy}^2M_{yy}M_{xx}-8M_{xy}^4)}{3M_{xx}^3+6M_{xy}^2M_{xx}+M_{yy}^2M_{xx}+2M_{xy}^2M_{yy}}M_{y\beta}$$

$$- \frac{4M_{xy}^3 + 3M_{xx}^2 M_{xy} + 3M_{yy}^2 M_{xy} + 2M_{xx}M_{yy}M_{xy}}{3M_{xx}^3 + 6M_{xy}^2 M_{xx} + M_{yy}^2 M_{xx} + 2M_{xy}^2 M_{yy}}$$
$$\times \left(\frac{3}{4} g_x^2 M_{x\beta} + \frac{1}{4} g_y^2 M_{x\beta} + \frac{1}{2} g_x g_y M_{y\beta} + \frac{1}{2}(3M_{xx} + M_{yy}) M_{x\beta} + M_{xy} M_{y\beta} \right) \Bigg\} \Bigg] \, \mathrm{d}\boldsymbol{g}\mathrm{d}\boldsymbol{k}. \tag{A 24}$$

To carry out the integrations over $\boldsymbol{g}$, we need the following results:

$$\int (\boldsymbol{g}\cdot\boldsymbol{k})^3 \exp\left\{-\frac{1}{4} g_a M_{ab}^{-1} g_b\right\} \mathrm{d}\boldsymbol{g} = 16\pi^{1/2} |\boldsymbol{M}|^{1/2} \vartheta^{3/2}, \tag{A 25}$$

$$\int g_x^2 (\boldsymbol{g}\cdot\boldsymbol{k})^3 \exp\left\{-\frac{1}{4} g_a M_{ab}^{-1} g_b\right\} \mathrm{d}\boldsymbol{g} = 128\pi^{1/2} |\boldsymbol{M}|^{1/2} \vartheta^{1/2} \left[\{\vartheta k_x + \varpi k_y\}^2 + \frac{1}{4} |\boldsymbol{M}| k_y^2 \right], \tag{A 26}$$

$$\int g_x g_y (\boldsymbol{g}\cdot\boldsymbol{k})^3 \exp\left\{-\frac{1}{4} g_a M_{ab}^{-1} g_b\right\} \mathrm{d}\boldsymbol{g}$$
$$= 128\pi^{1/2} |\boldsymbol{M}|^{1/2} \vartheta^{1/2} [\{\vartheta k_x + \varpi k_y\}\{\vartheta k_y - \varpi k_x\} - \frac{1}{4} |\boldsymbol{M}| k_x k_y], \tag{A 27}$$

$$\int g_y^2 (\boldsymbol{g}\cdot\boldsymbol{k})^3 \exp\left\{-\frac{1}{4} g_a M_{ab}^{-1} g_b\right\} \mathrm{d}\boldsymbol{g} = 128\pi^{1/2} |\boldsymbol{M}|^{1/2} \vartheta^{1/2} \left[\{\vartheta k_y - \varpi k_x\}^2 + \frac{1}{4} |\boldsymbol{M}| k_x^2 \right], \tag{A 28}$$

$$\int g_x (\boldsymbol{g}\cdot\boldsymbol{k})^2 \exp\left\{-\frac{1}{4} g_a M_{ab}^{-1} g_b\right\} \mathrm{d}\boldsymbol{g} = 16\pi^{1/2} |\boldsymbol{M}|^{1/2} \vartheta^{1/2} \{\vartheta k_x + \varpi k_y\}, \tag{A 29}$$

$$\int g_y (\boldsymbol{g}\cdot\boldsymbol{k})^2 \exp\left\{-\frac{1}{4} g_a M_{ab}^{-1} g_b\right\} \mathrm{d}\boldsymbol{g} = 16\pi^{1/2} |\boldsymbol{M}|^{1/2} \vartheta^{1/2} \{\vartheta k_y - \varpi k_x\}, \tag{A 30}$$

$$\int g_x^3 (\boldsymbol{g}\cdot\boldsymbol{k})^2 \exp\left\{-\frac{1}{4} g_a M_{ab}^{-1} g_b\right\} \mathrm{d}\boldsymbol{g}$$
$$= \frac{32\pi^{1/2} |\boldsymbol{M}|^{1/2}}{\vartheta^{1/2}} \{\vartheta k_x + \varpi k_y\}[4\{\vartheta k_x + \varpi k_y\}^2 + 3|\boldsymbol{M}| k_y^2], \tag{A 31}$$

$$\int g_x^2 g_y (\boldsymbol{g}\cdot\boldsymbol{k})^2 \exp\left\{-\frac{1}{4} g_a M_{ab}^{-1} g_b\right\} \mathrm{d}\boldsymbol{g}$$
$$= \frac{32\pi^{1/2} |\boldsymbol{M}|^{1/2}}{\vartheta^{1/2}} [4\{\vartheta k_y - \varpi k_x\}\{\vartheta k_x + \varpi k_y\}^2 - 2|\boldsymbol{M}| k_x k_y \{\vartheta k_x + \varpi k_y\}$$
$$+ |\boldsymbol{M}| k_y^2 \{\vartheta k_y - \varpi k_x\}], \tag{A 32}$$

$$\int g_x g_y^2 (\boldsymbol{g}\cdot\boldsymbol{k})^2 \exp\left\{-\frac{1}{4} g_a M_{ab}^{-1} g_b\right\} \mathrm{d}\boldsymbol{g}$$
$$= \frac{32\pi^{1/2} |\boldsymbol{M}|^{1/2}}{\vartheta^{1/2}} [4\{\vartheta k_x + \varpi k_y\}\{\vartheta k_y - \varpi k_x\}^2 - 2|\boldsymbol{M}| k_x k_y \{\vartheta k_y - \varpi k_x\}$$
$$+ |\boldsymbol{M}| k_x^2 \{\vartheta k_x + \varpi k_y\}], \tag{A 33}$$

$$\int g_y^3 (\boldsymbol{g}\cdot\boldsymbol{k})^2 \exp\left\{-\frac{1}{4} g_a M_{ab}^{-1} g_b\right\} \mathrm{d}\boldsymbol{g}$$
$$= \frac{32\pi^{1/2} |\boldsymbol{M}|^{1/2}}{\vartheta^{1/2}} \{\vartheta k_y - \varpi k_x\}[4\{\vartheta k_y - \varpi k_x\}^2 + 3|\boldsymbol{M}| k_x^2], \tag{A 34}$$

where

$$\vartheta = \boldsymbol{k}\cdot\boldsymbol{M}\cdot\boldsymbol{k} = T(1-\eta\cos 2\theta) \quad \text{and} \quad \varpi = -T\eta\sin 2\theta, \tag{A 35a,b}$$

and the contact vector $\boldsymbol{k}$ (cf. figure 2) is given by

$$\boldsymbol{k} = \begin{bmatrix} \cos(\theta+\phi+\frac{1}{4}\pi) \\ \sin(\theta+\phi+\frac{1}{4}\pi) \end{bmatrix}. \tag{A 36}$$

Note that

$$(\vartheta k_x + \varpi k_y) = T[\cos(\theta+\phi+\tfrac{1}{4}\pi) - \eta\cos(\theta-\phi-\tfrac{1}{4}\pi)], \tag{A 37}$$

$$(\vartheta k_y - \varpi k_x) = T[\sin(\theta+\phi+\tfrac{1}{4}\pi) + \eta\sin(\theta-\phi-\tfrac{1}{4}\pi)], \tag{A 38}$$

and to within an error of $O(\eta^3)$ we have

$$\vartheta^{3/2} \approx T^{3/2}(1-\tfrac{3}{2}\eta\cos 2\theta + \tfrac{3}{8}\eta^2\cos^2 2\theta), \tag{A 39}$$

$$\vartheta^{1/2} \approx T^{1/2}(1-\tfrac{1}{2}\eta\cos 2\theta - \tfrac{1}{8}\eta^2\cos^2 2\theta), \tag{A 40}$$

$$\vartheta^{-1/2} \approx \frac{1+\frac{1}{2}\eta\cos 2\theta + \frac{3}{8}\eta^2\cos^2 2\theta}{T^{1/2}}. \tag{A 41}$$

Using the above results we can carry out the integrations over $\boldsymbol{g}$ and $\boldsymbol{k}$ to yield

$$\begin{aligned} I^{(1)}_{x\beta\beta} &= \frac{3\rho(1+e)^2T^{1/2}}{32\rho_p\sigma\pi^{1/2}(1+\eta^2+\eta^4)} \\ &\quad\times[\{96+114\eta^2+118\eta^4-7\eta^6+\eta\sin 2\phi(24-5\eta^2+20\eta^4)\}q_x \\ &\quad+\{\eta\cos 2\phi(-24+5\eta^2-20\eta^4)\}q_y], \end{aligned} \tag{A 42}$$

$$\begin{aligned} I^{(1)}_{y\beta\beta} &= \frac{3\rho(1+e)^2T^{1/2}}{32\rho_p\sigma\pi^{1/2}(1+\eta^2+\eta^4)}[\{\eta\cos 2\phi(-24+5\eta^2-20\eta^4)\}q_x \\ &\quad+\{96+114\eta^2+118\eta^4-7\eta^6-\eta\sin 2\phi(24-5\eta^2+20\eta^4)\}q_y], \end{aligned} \tag{A 43}$$

$$\begin{aligned} I^{(2)}_{x\beta\beta} &= -\frac{3\rho(1-e^2)T^{1/2}}{8\rho_p\sigma\pi^{1/2}(1+\eta^2+\eta^4)}[\{16+21\eta^2+21\eta^4-\eta^6+2\eta(1-\eta^2)^2\sin 2\phi\}q_x \\ &\quad+\{-2\eta(1-\eta^2)^2\cos 2\phi\}q_y], \end{aligned} \tag{A 44}$$

$$\begin{aligned} I^{(2)}_{y\beta\beta} &= -\frac{3\rho(1-e^2)T^{1/2}}{8\rho_p\sigma\pi^{1/2}(1+\eta^2+\eta^4)}[\{-2\eta(1-\eta^2)^2\cos 2\phi\}q_x \\ &\quad+\{16+21\eta^2+21\eta^4-\eta^6-2\eta(1-\eta^2)^2\sin 2\phi\}q_y], \end{aligned} \tag{A 45}$$

$$\begin{aligned} I^{(3)}_{x\beta\beta} &= -\frac{\rho(1+e)T^{1/2}}{32\rho_p\sigma\pi^{1/2}(1+\eta^2+\eta^4)} \\ &\quad\times[\{704+804\eta^2+933\eta^4+73\eta^6+\eta\sin 2\phi(208+157\eta^2+184\eta^4+105\eta^6)\}q_x \\ &\quad+\{-\eta\cos 2\phi(208+157\eta^2+184\eta^4+105\eta^6)\}q_y], \end{aligned} \tag{A 46}$$

$$\begin{aligned} I^{(3)}_{y\beta\beta} &= -\frac{\rho(1+e)T^{1/2}}{32\rho_p\sigma\pi^{1/2}(1+\eta^2+\eta^4)}[\{-\eta\cos 2\phi(208+157\eta^2+184\eta^4+105\eta^6)\}q_x \\ &\quad+\{704+804\eta^2+933\eta^4+73\eta^6-\eta\sin 2\phi(208+157\eta^2+184\eta^4+105\eta^6)\}q_y]. \end{aligned} \tag{A 47}$$

Substituting (A 42)–(A 47) into (A 14), we obtain the final expressions (6.13)–(6.15) for the third-order source term.

Appendix B. Series representation for collision integrals

Recall from § 3.2 that the integration over the contact vector $\boldsymbol{k}$ is transformed into the integration over another variable $\theta \in (0, 2\pi)$ (the angle between $\boldsymbol{k}$ and $|M_1\rangle$, the eigenvector corresponding to the smaller eigenvalue of the second-moment tensor $\boldsymbol{M}$; cf. figure 2). The expressions for the integrals appearing in (3.27)–(3.29) are

$$\mathscr{H}_{\alpha\beta\gamma}(\eta, R, \phi) \equiv \int_0^{2\pi} \cos^\alpha 2\theta \sin^\beta 2\theta\, (1-\eta\cos 2\theta)^{\gamma/2} \mathfrak{F}(\eta, R, \phi, \theta)\, \mathrm{d}\theta, \tag{B 1}$$

$$\mathscr{J}_{\alpha\beta\gamma}(\eta, R, \phi) \equiv \int_0^{2\pi} \cos^\alpha 2\theta \sin^\beta 2\theta\, (1-\eta\cos 2\theta)^{\gamma/2} \mathfrak{G}(\eta, R, \phi, \theta)\, \mathrm{d}\theta. \tag{B 2}$$

Now substituting the infinite series representation for $\mathfrak{F}$ and $\mathfrak{G}$, as given in (4.1) and (4.2), into above integrals, a term-by-term integration can be carried out for both integrals $\mathscr{H}_{\alpha\beta\gamma}$ and $\mathscr{J}_{\alpha\beta\gamma}$. For example, the series representation for $\mathscr{H}_{003}$ is

$$\begin{aligned}\mathscr{H}_{003}(\eta, R, \phi) &= 3\pi^{3/2}\eta R\cos 2\phi + \sum_{n=0}^{\infty} \Lambda(\tfrac{3}{2}, 2n)\pi^{1/2}\eta^{2n}\frac{2\Gamma(n+\frac{1}{2})}{n!} \\ &\quad + 12R^2\sum_{n=0}^{\infty}\Lambda\left(\frac{1}{2}, 2n\right)\eta^{2n}\frac{\pi^{1/2}(1+n+n\cos 4\phi)\Gamma(n+\frac{1}{2})}{(n+1)!} \\ &\quad + 8R^4\left[\frac{3}{4}\pi + \frac{3}{64}\pi\eta^2(3+2\cos 4\phi) + O(\eta^4)\right] + O(R^6),\end{aligned} \tag{B 3}$$

$$\begin{aligned}\mathscr{J}_{020}(\eta, R, \phi) &= \frac{1}{2}\pi^{3/2} - 4R\sum_{n=0}^{\infty}\Lambda(2n+\frac{1}{2}, 2n+1)\eta^{2n+1}\frac{\pi^{1/2}\cos 2\phi\,\Gamma(n+\frac{3}{2})}{(n+2)!} \\ &\quad + 2\pi R^2\sum_{n=0}^{\infty}\eta^{2n}\frac{\{2+n+(n-1)\cos 4\phi\}\Gamma(n+\frac{1}{2})}{(n+2)!} \\ &\quad - \frac{8}{3}R^3\sum_{n=0}^{\infty}\Lambda\left(2n+\frac{3}{2}, 2n+1\right)\eta^{2n+1} \\ &\quad \frac{\pi^{1/2}\cos 2\phi\{6+n+(n-3)\cos 4\phi\}\Gamma(n+\frac{3}{2})}{(n+3)!} + O(R^5),\end{aligned} \tag{B 4}$$

where

$$\Lambda(\alpha, \beta) \equiv \frac{\Gamma(\alpha+1)}{\beta!\Gamma(\alpha+1-\beta)}, \tag{B 5}$$

with similar expressions for other integrals of $\mathscr{H}_{\alpha\beta\gamma}$ and $\mathscr{J}_{\alpha\beta\gamma}$.

Each of the above infinite series at the third-order approximation in R and η, with error $O(R^m\eta^n)$ and $(m+n) \geqslant 4$, can be simplified to

$$\left.\begin{aligned}&\mathscr{H}_{003}(\eta, R, \phi) = 2\pi + 12\pi R^2 + 3\pi^{3/2}\eta R\cos 2\phi + \tfrac{3}{8}\pi\eta^2 + O(R^m\eta^n), \\ &\mathscr{H}_{103}(\eta, R, \phi) = -3\pi^{3/2}R\cos 2\phi - \tfrac{3}{2}\pi\eta \underbrace{- 6\pi^{3/2}R^3\cos 2\phi - \tfrac{3}{2}\pi\eta R^2(2+\cos 4\phi)}, \\ &\mathscr{H}_{013}(\eta, R, \phi) = 3\pi^{3/2}R\sin 2\phi + \underbrace{6\pi^{3/2}R^3\sin 2\phi + \tfrac{3}{2}\pi\eta R^2\sin 4\phi}, \\ &\mathscr{H}_{021}(\eta, R, \phi) = \pi - \tfrac{1}{32}\pi\eta^2 + 3\pi R^2(2-\cos 4\phi), \\ &\mathscr{H}_{111}(\eta, R, \phi) = -3\pi R^2\sin 4\phi,\end{aligned}\right\} \tag{B 6}$$

$$\left.\begin{aligned}
\mathscr{J}_{020}(\eta, R, \phi) &= \tfrac{1}{2}\pi^{3/2} - \tfrac{1}{2}\pi R\eta\cos 2\phi + \pi^{3/2}R^2(2-\cos 4\phi),\\
\mathscr{J}_{110}(\eta, R, \phi) &= \tfrac{1}{2}\pi R\eta\sin 2\phi - \pi^{3/2}R^2\sin 4\phi,\\
\mathscr{J}_{010}(\eta, R, \phi) &= 4\pi R\sin 2\phi - \underbrace{\pi^{3/2}\eta R^2\sin 4\phi + \tfrac{3}{8}\pi R\eta^2\sin 2\phi + 4\pi R^3\sin 2\phi}, \\
\mathscr{J}_{200}(\eta, R, \phi) &= \tfrac{1}{2}\pi^{3/2} - \tfrac{3}{2}\pi R\eta\cos 2\phi + \pi^{3/2}R^2(2+\cos 4\phi),\\
\mathscr{J}_{100}(\eta, R, \phi) &= -4\pi R\cos 2\phi + \underbrace{\pi^{3/2}\eta R^2(2+\cos 4\phi) - \tfrac{9}{8}\pi R\eta^2\cos 2\phi - 4\pi R^3\cos 2\phi},
\end{aligned}\right\} \quad \text{(B 7)}$$

$$\left.\begin{aligned}
\mathscr{J}_{102}(\eta, R, \phi) &= -4\pi R\cos 2\phi - \tfrac{1}{2}\pi^{3/2}\eta + \underbrace{\tfrac{3}{8}\pi R\eta^2\cos 2\phi - 4\pi R^3\cos 2\phi},\\
\mathscr{J}_{012}(\eta, R, \phi) &= 4\pi R\sin 2\phi - \underbrace{\tfrac{1}{8}\pi R\eta^2\sin 2\phi + 4\pi R^3\sin 2\phi},\\
\mathscr{J}_{002}(\eta, R, \phi) &= \pi^{3/2} + 4R^2\pi^{3/2} + 2\pi\eta R\cos 2\phi.
\end{aligned}\right\} \quad \text{(B 8)}$$

Removing the underbraced terms yields second-order series approximation for the above integral expressions. Note that some of the above quantities have zero contribution at third order, and hence they are equal at both second- and third-order approximation.

Appendix C. Evaluation of stress tensor for uniform shear flow

Here we present explicit expressions for the transport coefficients of the USF as obtained from series solutions. The components of the dimensionless stress tensor are

$$\begin{aligned}
P^*_{xx} &= \frac{P_{xx}}{\rho_p {U_R}^2}\\
&= \nu T^*\left((1+\eta\sin 2\phi) + \frac{\nu g_0(1+e)}{\pi^{3/2}}[\mathscr{J}_{002}(\eta, R, \phi)\right.\\
&\quad \left. - \cos 2\phi\,\mathscr{J}_{012}(\eta, R, \phi) - \sin 2\phi\,\mathscr{J}_{102}(\eta, R, \phi)]\right), \qquad \text{(C 1)}\\
P^*_{yy} &= \frac{P_{yy}}{\rho_p {U_R}^2}\\
&= \nu T^*\left((1-\eta\sin 2\phi) + \frac{\nu g_0(1+e)}{\pi^{3/2}}[\mathscr{J}_{002}(\eta, R, \phi)\right.\\
&\quad \left. + \cos 2\phi\,\mathscr{J}_{012}(\eta, R, \phi) + \sin 2\phi\,\mathscr{J}_{102}(\eta, R, \phi)]\right), \qquad \text{(C 2)}\\
P^*_{xy} &= \frac{P_{xy}}{\rho_p {U_R}^2}\\
&= \nu T^*\left(-\eta\cos 2\phi + \frac{\nu g_0(1+e)}{\pi^{3/2}}[\cos 2\phi\,\mathscr{J}_{102}(\eta, R, \phi) - \sin 2\phi\,\mathscr{J}_{012}(\eta, R, \phi)]\right), \qquad \text{(C 3)}
\end{aligned}$$

where ρ_p is the density of particles, and the reference velocity scale for non-dimensionalization is $U_R = 2\dot{\gamma}\sigma$. Substituting the power-series expressions for $\mathscr{J}_{002}$, $\mathscr{J}_{012}$ and $\mathscr{J}_{102}$ as given by (B 8) in appendix B, we obtain the super-Burnett-order, $O(R^3)$, expression for the stress tensor in § 4.2.

The pressure $p = (P_{xx} + P_{yy})/2$ is calculated from the average of (C 1) and (C 2), which can be further decomposed into its kinetic and collisional parts:

$$p^* = \frac{p}{\rho_p {U_R}^2} = p_k^* + p_c^* = \nu T^* \left[1 + \frac{\nu g_0 (1+e)}{\pi^{3/2}} \mathscr{J}_{002}(\eta, R, \phi)\right], \tag{C 4}$$

$$p_k^* = \nu T^*, \tag{C 5}$$

$$p_c^* = \frac{\nu g_0 (1+e)}{\pi^{3/2}} T^* \mathscr{J}_{002}(\eta, R, \phi). \tag{C 6}$$

The dimensionless shear viscosity and its kinetic and collisional components are given by

$$\begin{aligned} \mu^* &= \frac{-P_{xy}}{\rho_p {U_R}^2} = \mu_k^* + \mu_c^* \\ &= \frac{\nu}{64R^2}\left[\eta \cos 2\phi - \frac{\nu g_0 (1+e)}{\pi^{3/2}} \{\cos 2\phi\, \mathscr{J}_{102}(\eta, R, \phi) - \sin 2\phi\, \mathscr{J}_{012}(\eta, R, \phi)\}\right], \end{aligned} \tag{C 7}$$

$$\mu_k^* = \frac{\nu \eta \cos 2\phi}{64R^2}, \tag{C 8}$$

$$\mu_c^* = -\frac{\nu^2 g_0 (1+e)}{64\pi^{3/2}R^2}[\cos 2\phi\, \mathscr{J}_{102}(\eta, R, \phi) - \sin 2\phi\, \mathscr{J}_{012}(\eta, R, \phi)]. \tag{C 9}$$

The granular temperature (3.5) is given by

$$T = \frac{M_{xx} + M_{yy}}{2} \quad \Longrightarrow \quad T^* = \frac{T}{{U_R}^2} = \frac{1}{64R^2}. \tag{C 10}$$

For the full numerical solution of the moment equations (3.29)–(3.31), the transport coefficients are calculated from (C 1)–(C 9) by evaluating the integrals $\mathscr{J}_{002}$, $\mathscr{J}_{102}$ and $\mathscr{J}_{012}$ in (B 2) by using standard quadrature rules.

On the other hand, for the series solution, (4.3) or (4.4) (at second order or third order, respectively) are solved for η, R and ϕ. Next the series expressions for $\mathscr{J}_{002}$, $\mathscr{J}_{102}$ and $\mathscr{J}_{012}$ ((B 8) from appendix B) are inserted into (C 1)–(C 9) in order to calculate the transport coefficients.

Appendix D. Constitutive model of Navier–Stokes order (Lutsko 2005)

The constitutive model for an inelastic hard-disk system is taken from Lutsko (2005), which is almost identical to that of Garzo *et al.* (2007) up to the first Sonine approximation:

$$g_0 = \frac{16 - 7\nu}{16(1-\nu)^2}, \tag{D 1}$$

$$\alpha_2 = \frac{16(1-e)(1-2e^2)}{57 - 25e + 30(1-e)e^2}, \tag{D 2}$$

$$\varphi_\mu^* = g_0\left(1 - \tfrac{1}{8}(1-e)(1-3e)\right), \tag{D 3}$$

$$\zeta^* = \tfrac{1}{2} g_0 (1 - e^2). \tag{D 4}$$

The dimensionless pressure with its kinetic and collisional parts are given by

$$p^* = \nu T^*(1 + (1+e)\nu g_0) = p_k^* + p_c^*, \tag{D 5}$$

$$p_k^* = \nu T^*, \tag{D 6}$$

$$p_c^* = (1+e)\nu^2 g_0 T^*, \tag{D 7}$$

and the dimensionless viscosity is

$$\mu^* = \mu_k^* + \mu_c^*, \tag{D 8}$$

$$\mu_k^* = \frac{\sqrt{\pi}}{8} T^{*1/2} \frac{(1 - \frac{1}{4}(1+e)(1-3e)\nu g_0)}{(\varphi_\mu^* - \frac{1}{2}\zeta^*)}, \tag{D 9}$$

$$\mu_c^* = \frac{\sqrt{\pi}}{8} T^{*1/2} \left[\frac{(1+e)\{1 - \frac{1}{4}(1+e)(1-3e)\nu g_0\}\nu g_0}{2(\varphi_\mu^* - \frac{1}{2}\zeta^*)} + \frac{4(1+e)(1 - \frac{1}{16}\alpha_2)\nu^2 g_0}{\pi} \right]. \tag{D 10}$$

The expression for the dimensionless temperature follows from the energy balance equation:

$$T^* = \frac{\pi(1 - \frac{1}{4}(1+e)(1-3e)\nu g_0)(1 + \frac{1}{2}(1+e)\nu g_0)}{32(1-e^2)(1 + \frac{3}{16}\alpha_2)(\varphi_\mu^* - \frac{1}{2}\zeta^*)\nu^2 g_0} + \frac{1 - \frac{1}{16}\alpha_2}{8(1-e)(1 + \frac{3}{16}\alpha_2)}. \tag{D 11}$$

REFERENCES

ALAM, M. & LUDING, S. 2003*a* First normal stress difference and crystallization in sheared granular fluid. *Phys. Fluids* **15**, 2298–2312.

ALAM, M. & LUDING, S. 2003*b* Rheology of bidisperse granular mixtures via event-driven simulations. *J. Fluid Mech.* **476**, 69–103.

ALAM, M. & LUDING, S. 2005*a* Energy non-equipartition, rheology and microstructure in sheared bidisperse granular mixtures. *Phys. Fluids* **17**, 063303.

ALAM, M. & LUDING, S. 2005*b* Non-Newtonian granular fluid: simulation and theory. In *Powders and Grains* (ed. R. Garcia-Rojo, H. J. Herrmann & S. McNamara), pp. 1141–1144. A. A. Balkema.

ALAM, M., WILLITS, J. T., ARNARSON, B. O. & LUDING, S. 2002 Kinetic theory of a binary mixture of nearly elastic disks with size and mass disparity. *Phys. Fluids* **14**, 4085–4087.

ARAKI, S. & TREMAINE, S. 1986 The dynamics of dense particle disks. *Icarus* **65**, 83–109.

BREY, J. J., DUFTY, J. W., KIM, C. S. & SANTOS, A. 1998 Hydrodynamics for granular flow at low density. *Phys. Rev.* E **58**, 4638–4653.

BRILLIANTOV, N. V. & PÖSCHEL, T. 2003 Hydrodynamics and transport coefficients for dilute granular gases. *Phys. Rev.* E **67**, 061304.

BRILLIANTOV, N. V. & PÖSCHEL, T. 2004 *Kinetic Theory of Granular Gases*. Oxford University Press.

BURNETT, D. 1935 The distribution of velocities in a slightly non-uniform gas. *Proc. Lond. Math. Soc.* **39**, 385–430.

CHAPMAN, S. & COWLING, T. G. 1970 *The Mathematical Theory for Non-Uniform Gases*. Cambridge University Press.

CHOU, C. S. & RICHMAN, M. W. 1998 Constitutive theory for homogeneous granular shear flows of highly inelastic spheres. *Physica* A **259**, 430–448.

ESPOSITO, L. 2006 *Planetary Rings*. Cambridge University Press.

GARZO, V. 2012 Grad's moment method for a low density granular gas: Navier–Stokes transport coefficients. *AIP Conf. Proc.* **1501**, 1031–1037.

GARZO, V., SANTOS, A. & MONTANERO, J. M. 2007 Modified Sonine approximation for the Navier–Stokes transport coefficients of a granular gas. *Physica* A **376**, 94–107.

GAYEN, B. & ALAM, M. 2006 Algebraic and exponential instabilities in a sheared micropolar granular fluid. *J. Fluid Mech.* **567**, 195–231.

GAYEN, B. & ALAM, M. 2008 Orientational correlation and velocity distributions in uniform shear flow of a dilute granular gas. *Phys. Rev. Lett.* **100**, 068002.

GOLDHIRSCH, I. 2003 Rapid granular flows. *Annu. Rev. Fluid Mech.* **35**, 267–293.

GOLDREICH, P. & TREMAINE, S. 1978 The velocity dispersion in Saturn's rings. *Icarus* **34**, 227–239.

GRAD, H. 1949 On the kinetic theory of rarefied gases. *Commun. Pure Appl. Maths* **2**, 331–407.

JENKINS, J. T. & RICHMAN, M. W. 1985*b* Grad's 13-moment system for a dense gas of inelastic spheres. *Arch. Rat. Mech. Anal.* **87**, 355–377.

JENKINS, J. T. & RICHMAN, M. W. 1985*a* Kinetic theory of plane flows of a dense gas of identical, rough, inelastic, circular disks. *Phys. Fluids* **28**, 3485–3494.

JENKINS, J. T. & RICHMAN, M. W. 1988 Plane simple shear of smooth inelastic circular disks. *J. Fluid Mech.* **192**, 313–328.

KOGAN, M. N. 1969 *Rarefied Gas Dynamics*. Plenum Press.

KREMER, G. M. & MARQUES, W. 2011 Fourteen moment theory for granular gases. *Kinet. Relat. Models* **4**, 317–331.

LATTER, H. N. & OGILVIE, G. I. 2006 The linear stability of dilute particulate rings. *Icarus* **184**, 498–516.

LEES, A. W. & EDWARDS, S. 1972 The computer study of transport processes under extreme conditions. *J. Phys.* C **5**, 1921–1929.

LUTSKO, J. F. 2004 Rheology of dense polydisperse granular fluids under shear. *Phys. Rev.* E **70**, 061101.

LUTSKO, J. F. 2005 Transport properties of dense dissipative hard-sphere fluids for arbitrary energy loss models. *Phys. Rev.* E **72**, 021306.

MITARAI, N. & NAKANISHI, H. 2007 Velocity correlations in dense granular shear flows: effects on energy dissipation and normal stress. *Phys. Rev.* E **75**, 031305.

MITARAI, N., NAKANISHI, H. & HAYAKAWA, H. 2002 Collisional granular flow as a micropolar fluid. *Phys. Rev. Lett.* **88**, 174301.

MONTANERO, J. M., GARZO, V., ALAM, M. & LUDING, S. 2006 Rheology of two- and three-dimensional granular mixtures under uniform shear flow: Enskog kinetic theory versus molecular dynamics simulations. *Granul. Matt.* **8**, 103–115.

RAO, K. K. R. & NOTT, P. R. 2008 *An Introduction to Granular Flow*. Cambridge University Press.

RONGALI, R. & ALAM, M. 2014 Higher-order effects on orientational correlation and relaxation dynamics in homogeneous cooling of a rough granular gas. *Phys. Rev.* E **89**, 062201.

ROSENAU, P. 1989 Extending hydrodynamics via the regularization of the Chapman–Enskog expansion. *Phys. Rev.* A **40**, 7193–7196.

SAHA, S. & ALAM, M. 2014 Conductivity and Dufour tensors in a sheared granular gas (in preparation).

SANTOS, A. 2008 Does the Chapman–Enskog expansion for sheared granular gases converge? *Phys. Rev. Lett.* **100**, 078003.

SANTOS, A., GARZO, V. & DUFTY, J. W. 2004 Inherent rheology of a granular fluid in uniform shear. *Phys. Rev.* E **69**, 061303.

SAVAGE, S. B. & JEFFREY, D. J. 1981 The stress tensor in a granular flow at high shear rates. *J. Fluid Mech.* **110**, 255–272.

SCHMIDT, J., SALO, H., SPAHN, F. & PETZSCHMANN, O. 2001 Viscous overstability in Saturn's B-ring: hydrodynamic theory and comparison to simulations. *Icarus* **153**, 316–331.

SELA, N. & GOLDHIRSCH, I. 1998 Hydrodynamic equations for rapid flows of smooth inelastic spheres. *J. Fluid Mech.* **361**, 41–74.

SELA, N., GOLDHIRSCH, I. & NOSKOWICZ, S. H. 1996 Kinetic theoretical study of a simply sheared two-dimensional granular gas to Burnett order. *Phys. Fluids* **8**, 2337–2353.

SHUKHMAN, G. 1984 Collisional dynamics of particles in Saturn's rings. *Sov. Astron.* **28**, 547–584.

SHUKLA, P. & ALAM, M. 2009 Order parameter description of shear-banding in granular Couette flow via Landau equation. *Phys. Rev. Lett.* **103**, 068001.

SHUKLA, P. & ALAM, M. 2011*a* Nonlinear stability and patterns in granular plane Couette flow: Hopf and pitchfork bifurcations, and evidence for resonance. *J. Fluid Mech.* **672**, 147–195.

SHUKLA, P. & ALAM, M. 2011*b* Weakly nonlinear theory of shear-banding instability in granular plane Couette flow: analytical solution, comparison with numerics and bifurcation. *J. Fluid Mech.* **666**, 204–253.

SIMON, V. & JENKINS, J. T. 1994 On the vertical structure of dilute planetary rings. *Icarus* **110**, 109–116.

TORRILHON, M. & STRUCHTRUP, H. 2004 Regularized 13-moment equations: shock structure calculations and comparison to Burnett models. *J. Fluid Mech.* **513**, 171–198.

TRUESDELL, C. & MUNCASTER, R. G. 1980 *Fundamentals of Maxwell's Kinetic Theory of a Simple Monatomic Gas*. Academic Press.

VEGA REYES, F., SANTOS, A. & GARZO, V. 2013 Steady base states for non-Newtonian granular hydrodynamics. *J. Fluid Mech.* **719**, 431–464.

VERLET, L. & LEVESQUE, D. 1982 Integral equations for classical fluids III. The hard disk system. *Mol. Phys.* **46**, 969–980.